Original Study **Open Access**

Ashish Solanki*, Jitendra Kumar Sharma

Influence of Raft in the Analysis of Granular Piles

https://doi.org/10.2478/sgem-2025-0012
received December 17, 2024; accepted March 3, 2025.

Abstract: In an era marked by rapid growth and diminishing natural resources, including land, ground improvement has become imperative, particularly for civil engineers dealing with soft soils. This study explores the potential of granular piles (GPs) and granular piled rafts (GPRs) as cost-effective and sustainable solutions for overcoming resource-related challenges. The research focuses on a comparative analysis of the settlement interaction factor (SIF) within groups of GPRs and GPs as foundation systems. By evaluating and comparing the settlement magnification effects induced by adjacent foundation elements, the study aims to uncover insights into the influence of spacing and relative stiffness on the SIF. These findings offer valuable information for engineers, enabling them to optimize designs and address potential settlement-related issues in a resource-conscious manner

Keywords: settlement interaction factor (SIF); granular piled rafts (GPRs); granular piles (GPs).

1 Introduction

The SIF emerges as a linchpin in the evaluation of foundation systems featuring closely spaced elements. This study embarks on a rigorous exploration of the SIF within groups of granular piled rafts (GPRs) and granular piles (GPs), employing both meticulous rigorous (“R”) and insightful superposition (“S”) analyses. The overarching goal is to provide a comprehensive understanding of settlement magnification effects and the myriad factors influencing settlement interactions. The insights gleaned from this analysis contribute substantially to the reservoir of knowledge in geotechnical engineering, equipping engineers with the acumen needed for judicious design decisions in projects involving these intricate foundation systems.

2 Literature Review

The foundation for this study is meticulously laid on the bedrock of existing literature, case studies, and analytical methodologies. The trajectory begins with the seminal study by Mattes and Poulos in 1969, pioneering the use of GPs as a ground improvement technique. Since then, a cadre of researchers has made formidable contributions, enriching the landscape of knowledge and applications in this domain. Poorooshasb et al. (1998) delved into two types of columns, plain and reinforced (encased), proposing an upper bound analysis to discern the settlement nuances of foundation systems embracing stone column inclusions. The study ingeniously considered the non-linear behavior of surrounding soft clay, unraveling valuable insights into the settlement dynamics of such foundation systems. Sanctic and Mandolini (2006) devoted their efforts to calculate the bearing capacity of pile–raft foundations nestled in soft clay deposits. Merging experimental findings with three-dimensional numerical analyses, they established a discerning criterion for assessing the bearing capacity of pile–raft foundation systems. The study ingeniously employed hyperbolic non-linear elastic models to simulate the behavior of stone columns and soft soils, spotlighting the potential advantages of geosynthetic encasement in enhancing the performance of stone column systems. Tan et al. (2008) took a distinctive route, scrutinizing the acceleration of consolidation rates through stone columns using a fundamental unit cell approach. Analyzing the consolidation process surrounding a column within a cylindrical soil body, the study shed light on the enhanced consolidation characteristics achieved through the strategic deployment of stone columns. Zhang and Zhao (2015) presented analytical solutions based on the unit cell concept, predicting the deformation behavior of geotextile-encased stone columns at varying depths

***Corresponding author: Ashish Solanki,** PhD Research Scholar, Department of Civil Engineering, Rajasthan Technical University, Kota, Rajasthan, India, E-mail: asolanki.phd19@rtu.ac.in ; ashish92.4ueverback@gmail.com; ORCID: 0000-0003-3021-7967
Dr. Jitendra Kumar Sharma, Professor and HOD, Department of Civil Engineering, Rajasthan Technical University, Kota, Rajasthan, India; ORCID: 0000-0002-4584-6793

below the column's top plane. Offering analytical tools to assess the performance of such composite foundation systems, this study added another layer of understanding to the intricate dynamics of ground improvement. Najjar and Skeini (2015) turned their gaze to the load-carrying capacity improvement of reinforced ground with stone columns under both drained and undrained conditions. Their findings underscored higher percentage improvements in load-carrying capacity for undrained conditions than drained conditions. Furthermore, the study illuminated the economic practicality constraints associated with increasing the area replacement ratio beyond certain thresholds for drained conditions. Hong et al. (2016) delved into the effects of encasement stiffness and strength on the response of individual geotextile-encased granular columns embedded in soft soil through model tests. Employing similarity analysis to ensure comparable behavior between prototype-scale and model-scale columns, the study unraveled insights into the influence of encasement properties on the behavior of these composite foundation elements. Garg and Sharma (2019) undertook a numerical assessment of a partially stiffened group of floating GPs, concurrently evaluating the SIF. The SIF, an instrumental metric quantifying the interaction effects between adjacent piles within a group, was scrutinized to decipher how the presence of neighboring piles influences the settlement behavior of the group. Solanki et al. (2022) traversed the realm of continuum mechanics, employing a continuum approach to analyze the interaction between two floating GPRs. The goal was to quantify the magnitude of interaction effects between the two floating GPRs, thus advancing our understanding of piled–raft systems. Rathor and Sharma (2023) introduced a valuable perspective, positing that an annular raft proves more effective than a solid raft for water tanks, adding a nuanced layer to the understanding of raft configurations. Solanki and Sharma (2023) contributed an analytical analysis of a group of floating GPRs, focusing on unraveling how the presence of one piled–raft influences the performance and behavior of the adjacent piled–raft. This endeavor to explore the intricate dynamics of piled–raft interactions set the stage for the present study. The crux of the current research systematically dives into the interplay between key parameters α, K_{gp}, L/d, and s/d—in the context of granular piles, both with and without rafts. By meticulously unraveling the relationships among these factors, the study aspires to offer a profound understanding of the intricate dynamics of pile–raft interactions. The holistic approach of the present study, encompassing both individual piles and those supported by rafts, sets it apart. This comprehensive exploration contributes to a nuanced and detailed understanding of the factors influencing the performance of foundation systems.

3 Problem Understanding and Analytical Approach

3.1 Assumptions made during analysis:

- Elastic Continuum Approach: The analysis assumes the elastic continuum approach, which considers the soil and structures as continuous and elastic materials. This assumption neglects any discontinuities or non-linear behavior that may exist in the actual system.
- Homogeneous and Isotropic Soil: The soil surrounding the granular pile is assumed to be homogeneous, meaning it has consistent properties throughout the analyzed area. Additionally, it is assumed to be isotropic, meaning its properties are the same in all directions. These assumptions simplify the analysis but may not accurately represent the actual soil conditions.
- Linear Elastic Behavior: The soil is assumed to exhibit linear elastic behavior and has a linear stress–strain relationship. This assumption is commonly made in many geotechnical analyses.
- Smooth and Rigid Base of the Granular Pile: The base of the granular pile is assumed to be smooth and rigid. This assumption implies that there is no slip or deformation at the pile–soil interface and simplifies the analysis. However, in reality, the pile–soil interaction may involve some degree of roughness, friction, or non-rigid behavior at the interface.

The problem addressed in this study involves the analysis of a group of GPRs and a group of GPs under the influence of an axial load, denoted as "P." The GPs have a length of "L" and a diameter of "d" (where "d = 2a") and are spaced at a ratio of "s/d," which are illustrated in Figs. 1 and 3. Stresses on any i^{th} element of the GP are shown in Fig. 2. The discretization scheme for the GP and the rigid raft of diameter "D" are shown in Figs. 5 and 6. The analysis is conducted using the elastic continuum approach. The soil properties considered in the analysis are the modulus of deformation (E_s) and Poisson's ratio (ν_s). Similarly, the granular pile properties are characterized by the modulus of deformation (E_{gp}) and Poisson's ratio (ν_{gp}). The relative stiffness of the granular pile, denoted as K_{gp}, is defined as the ratio of the modulus of deformation of the granular pile

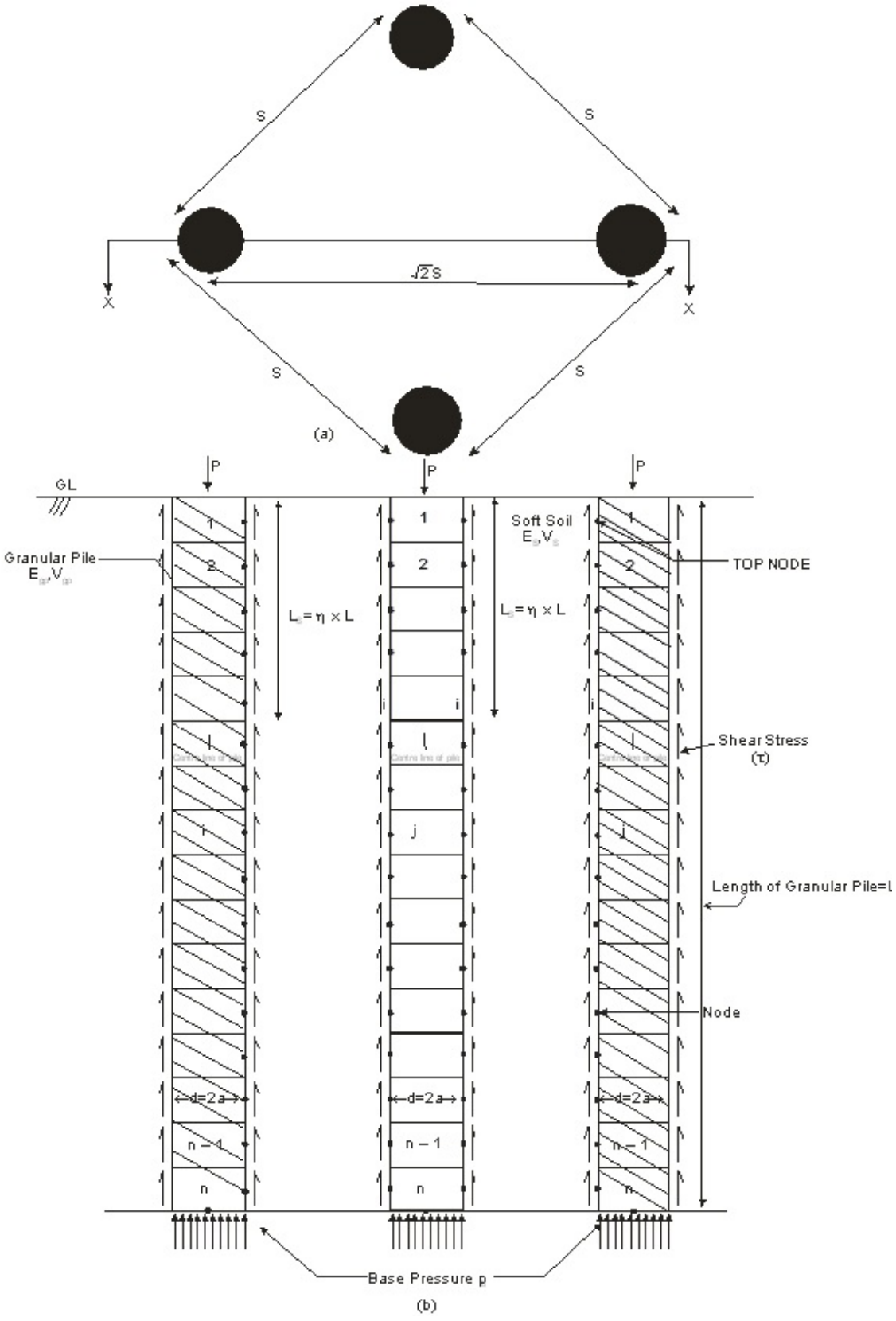

Figure 1: (a) Layout of a cluster consisting of four floating granular piles (GPs) arranged symmetrically. (b) Sectional elevation at X–X of a cluster comprising four symmetrically positioned floating GPs (Garg and Sharma, 2019).

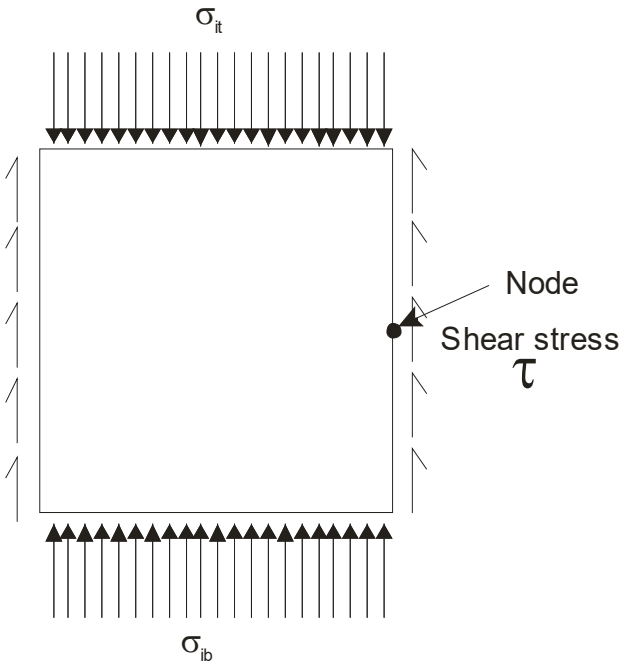

Figure 2: Stresses on any i^{th} element of the GP.

to that of the soil ($K_{gp} = E_{gp}/E_s$). Additionally, the pressure applied to the base of the granular pile is assumed to be uniform and represented as "p_b," as shown in Fig. 4

3.2 Displacements of Soil at GP Nodes

3.2.1 GPRs

Based on the study by Solanki et al. (2022), the equation describing soil displacement at nodes of a group of two GPRs is as follows:

1. Single GPR

$$\{\rho^{ps}\} = \left\{\frac{S^{ps}}{d}\right\} = \left[I_1^{ppf}\right]\left\{\frac{\tau}{E_s}\right\} + \left[I_1^{prf}\right]\left\{\frac{p_r}{E_s}\right\} \quad (1)$$

2. Two GPRs

$$\{\rho^{ps}\} = \left\{\frac{S^{ps}}{d}\right\} = \left[\left[I_1^{ppf}\right] + \left[I_2^{ppf}\right]\right]\left\{\frac{\tau}{E_s}\right\} + \left[\left[I_1^{prf}\right] + \left[I_2^{prf}\right]\right]\left\{\frac{p_r}{E_s}\right\} \quad (2)$$

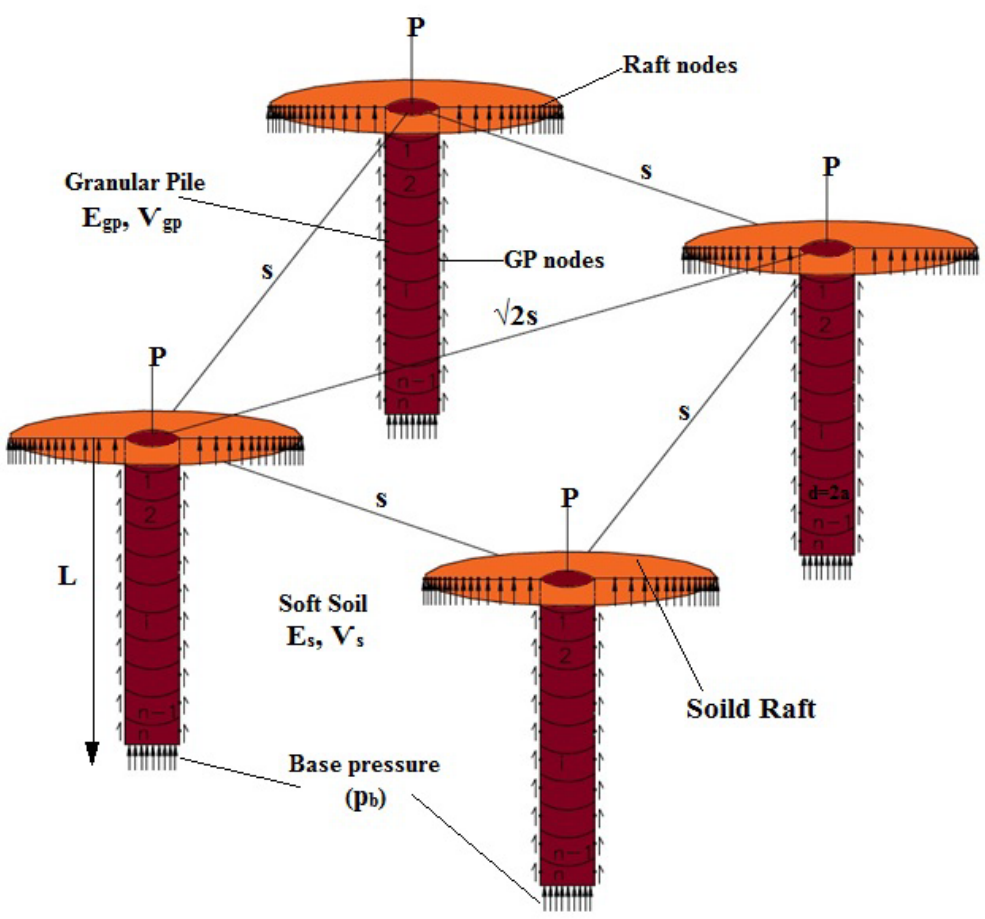

Figure 3: Four floating GPRs units

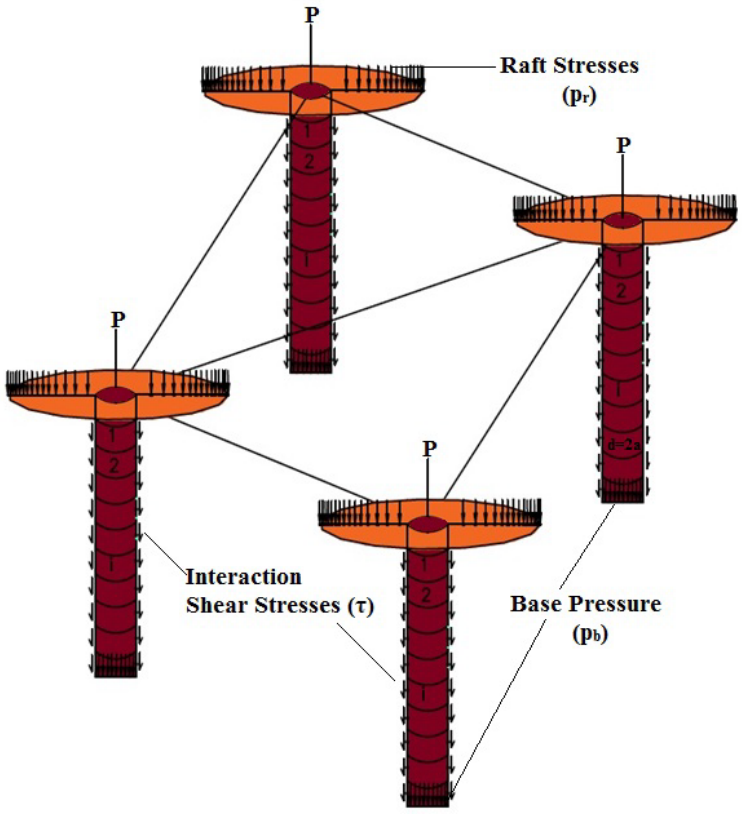

Figure 4: Soil stresses in the four floating GPR units

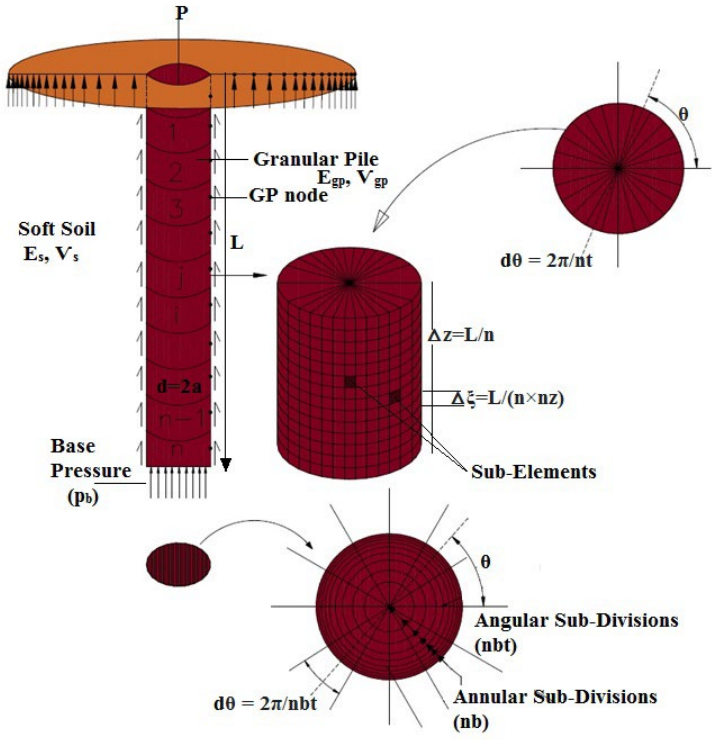

Figure 5: Numerical integration discretization scheme for GP.

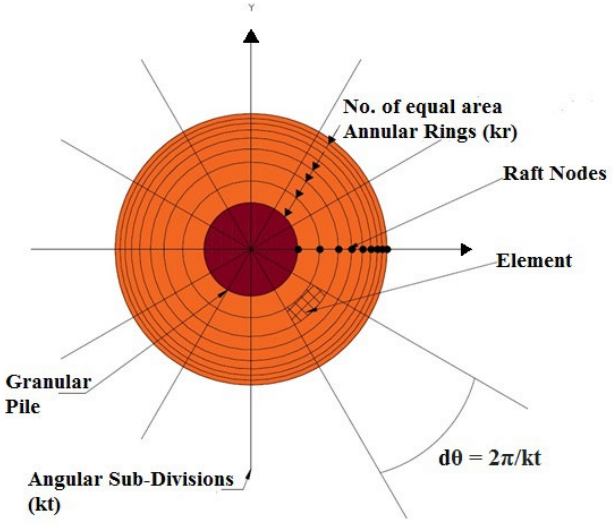

Figure 6: Discretization scheme of solid raft (Solanki et al., 2022).

Based on the study by Solanki and Sharma (2023), the equation describing soil displacement at nodes of a group of three and four GPRs is as follows:
3. Three GPRs

$$\{\rho^{ps}\} = \left\{\frac{S^{ps}}{d}\right\} = \left[\left[I_1^{ppf}\right] + \left[I_2^{ppf}\right] + \left[I_3^{ppf}\right]\right]\left\{\frac{\tau}{E_s}\right\} + \\ + \left[\left[I_1^{prf}\right] + \left[I_2^{prf}\right] + \left[I_3^{prf}\right]\right]\left\{\frac{p_r}{E_s}\right\} \quad (3)$$

Due to symmetry of position of GPRs 2 and 3, eq. 3 can be written as follows:

$$\{\rho^{ps}\} = \left\{\frac{S^{ps}}{d}\right\} = \left[\left[I_1^{ppf}\right] + 2 \times \left[I_2^{ppf}\right]\right]\left\{\frac{\tau}{E_s}\right\} + \\ + \left[\left[I_1^{prf}\right] + 2 \times \left[I_2^{prf}\right]\right]\left\{\frac{p_r}{E_s}\right\} \quad (4)$$

4. Four GPRs

$$\{\rho^{ps}\} = \left\{\frac{S^{ps}}{d}\right\} = \left[\left[I_1^{ppf}\right] + \left[I_2^{ppf}\right] + \left[I_3^{ppf}\right] + \\ + \left[I_4^{ppf}\right]\right]\left\{\frac{\tau}{E_s}\right\} + \left[\left[I_1^{prf}\right] + \left[I_2^{prf}\right] + \left[I_3^{prf}\right] + \left[I_4^{prf}\right]\right]\left\{\frac{p_r}{E_s}\right\} \quad (5)$$

Due to symmetry of position of GPRs 2 and 3, eq. 5 can be written as follows:

$$\{\rho^{ps}\} = \left\{\frac{S^{ps}}{d}\right\} = \left[\left[I_1^{ppf}\right] + 2 \times \left[I_2^{ppf}\right] + \left[I_4^{ppf}\right]\right]\left\{\frac{\tau}{E_s}\right\} + \\ + \left[\left[I_1^{prf}\right] + 2 \times \left[I_2^{prf}\right] + \left[I_4^{prf}\right]\right]\left\{\frac{p_r}{E_s}\right\} \quad (6)$$

where $\{S^{ps}\}$ and $\{\rho^{ps}\}$ are vertical and normalized vertical soil displacements. $[I^{ppf}]_{(n+1)\times(n+1)}$ and $[I^{prf}]_{(n+1)\times kr}$ are displacement factor for the effect of GP shear stresses and base pressure and raft stresses on settlements of nodes of pile elements, respectively. {τ} and {pr} are column vectors of size {n+1} and {kr}.

3.3 Displacement of Soil at Raft Node Points

3.3.1 GPRs

Based on the study by Solanki et al. (2022), the equation describing soil displacement at raft nodes of a group of two GPRs is as follows:
1. Single GPR

$$\{\rho^{rs}\} = \left\{\frac{S^{rs}}{d}\right\} = \left[I_1^{rpf}\right]\left\{\frac{\tau}{E_s}\right\} + \left[I_1^{rrf}\right]\left\{\frac{p_r}{E_s}\right\} \quad (7)$$

2. Two GPRs

$$\{\rho^{rs}\} = \left\{\frac{S^{rs}}{d}\right\} = \left[\left[I_1^{rpf}\right] + \left[I_2^{rpf}\right]\right]\left\{\frac{\tau}{E_s}\right\} + \\ + \left[\left[I_1^{rrf}\right] + \left[I_2^{rrf}\right]\right]\left\{\frac{p_r}{E_s}\right\} \quad (8)$$

Based on the study by Solanki and Sharma (2023), the equation describing soil displacement at raft nodes of a group of three and four GPRs is as follows:
3. Three GPRs

$$\{\rho^{rs}\} = \left\{\frac{S^{rs}}{d}\right\} = \left[\left[I_1^{rpf}\right] + \left[I_2^{rpf}\right] + \\ + \left[I_3^{rpf}\right]\right]\left\{\frac{\tau}{E_s}\right\} + \left[\left[I_1^{rrf}\right] + \left[I_2^{rrf}\right] + \left[I_3^{rrf}\right]\right]\left\{\frac{p_r}{E_s}\right\} \quad (9)$$

Due to symmetry of position of GPRs 2 and 3, eq. 9 can be written as follows:

$$\{\rho^{rs}\} = \left\{\frac{S^{rs}}{d}\right\} = \left[\left[I_1^{rpf}\right] + 2 \times \left[I_2^{rpf}\right]\right]\left\{\frac{\tau}{E_s}\right\} + \\ + \left[\left[I_1^{rrf}\right] + 2 \times \left[I_2^{rrf}\right]\right]\left\{\frac{p_r}{E_s}\right\} \quad (10)$$

4. Four GPRs

$$\{\rho^{rs}\} = \left\{\frac{S^{rs}}{d}\right\} = \left[\left[I_1^{rpf}\right] + \left[I_2^{rpf}\right] + \left[I_3^{rpf}\right] + \\ + \left[I_4^{rpf}\right]\right]\left\{\frac{\tau}{E_s}\right\} + \left[\left[I_1^{rrf}\right] + \left[I_2^{rrf}\right] + \left[I_3^{rrf}\right] + \left[I_4^{rrf}\right]\right]\left\{\frac{p_r}{E_s}\right\} \quad (11)$$

Due to symmetry of position of GPRs 2 and 3, eq. 11 can be written as follows:

$$\{\rho^{rs}\} = \left\{\frac{S^{rs}}{d}\right\} = \left[\left[I_1^{rpf}\right] + 2 \times \left[I_2^{rpf}\right] + \right.$$
$$\left. + \left[I_4^{rpf}\right]\right]\left\{\frac{\tau}{E_s}\right\} + \left[\left[I_1^{rrf}\right] + 2 \times \left[I_2^{rrf}\right] + \left[I_4^{rrf}\right]\right]\left\{\frac{p_r}{E_s}\right\} \quad (12)$$

where $\{S^{rs}\}$ and $\{\rho^{rs}\}$ are vertical and normalized vertical soil displacements, $[I^{rpf}]_{kr\times(n+1)}$ and $[I^{rrf}]_{kr\times kr}$ are matrix of size kr×(n+1) and kr×kr respectively

3.3.2 GP Displacements

The vertical displacements of the nodes within the GP in relation to the shaft shear stresses evaluated by [9] are given by:

$$\{\rho^{pp}\} = \rho_t\{1\} + [D_1]\left\{\frac{\tau}{E_s}\right\} \quad (13)$$

where $[D_1]$ matrix of dimension (n+1), given by = $[B_1] \times [A_1]$.

3.3.3 Displacements of the Raft

In this analysis, as per the study by Solanki et al. (2022), "assuming the raft to be rigid, it leads to uniform displacements across all raft nodes. As a result, the settlement of the top of the granular pile, denoted as "ρ_t," is assumed to be equivalent to the displacement of the raft." This relationship can be expressed as follows:

$$\{\rho^{rr}\}=\rho_t\{1\} \quad (14)$$

Here, $\{\rho^{rr}\}$ denotes a vector that represents the displacements of rafts characterized by the size "kr."

3.4 Condition of Compatibility

3.4.1 Correlation between Displacements of the GP and the Soil

For a GPR, Eqs (1) and (13) are equated to establish a relationship $\{\rho^{ps}\}=\{\rho^{pp}\}$ or

$$[AA]\left\{\frac{\tau}{E_s}\right\} + \left[I_1^{ppf}\right]\left\{\frac{p_r}{E_s}\right\} = \rho_t\{1\} \quad (15)$$

where $[AA] = [I_1^{ppf}]$- $[D_1]$ of size (n+1) × (n+1).

For 2GPRs, Eqs (2) and (13) are equated to establish a relationship $\{\rho^{ps}\}=\{\rho^{pp}\}$ or

$$[AA_1]\left\{\frac{\tau}{E_s}\right\} + \left[\left[I_1^{prf}\right] + \left[I_2^{prf}\right]\right]\left\{\frac{p_r}{E_s}\right\} = \rho_t\{1\} \quad (16)$$

where $[AA_1] = [[I_1^{ppf}]+[I_2^{ppf}]$ - $[D_1]$ of size (n+1) × (n+1).

For 3GPRs, Eqs (4) and (13) are equated to establish a relationship $\{\rho^{ps}\}=\{\rho^{pp}\}$ or

$$[AA_2]\left\{\frac{\tau}{E_s}\right\} + \left[\left[I_1^{prf}\right] + 2 \times \left[I_2^{prf}\right]\right]\left\{\frac{p_r}{E_s}\right\} = \rho_t\{1\} \quad (17)$$

where $[AA_2] = [[I_1^{ppf}]+2\times[I_2^{ppf}]$ - $[D_1]$ of size (n+1) × (n+1).

For 4GPRs, Eqs (6) and (13) are equated to establish a relationship $\{\rho^{ps}\}=\{\rho^{pp}\}$ or

$$[AA_3]\left\{\frac{\tau}{E_s}\right\} + \left[\left[I_1^{prf}\right] + 2 \times \left[I_2^{prf}\right] + \left[I_4^{prf}\right]\right]\left\{\frac{p_r}{E_s}\right\} = \rho_t\{1\} \quad (18)$$

where $[AA_3] = [[I_1^{ppf}]+2\times[I_2^{ppf}]+[I_4^{ppf}]]$- $[D_1]$.

3.4.2 Concordance of Displacements between the Raft and the Soil

For a GPR, Eqs (7) and (14) are equated to establish a relationship $\{\rho^{rs}\}=\{\rho^{rr}\}$ or

$$\{\rho^{rs}\} = \left\{\frac{S^{rs}}{d}\right\} = \left[I_1^{rpf}\right]\left\{\frac{\tau}{E_s}\right\} + \left[I_1^{rrf}\right]\left\{\frac{p_r}{E_s}\right\} = \rho_t\{1\} \quad (19)$$

For a group of two GPRs, Eqs (8) and (14) are equated as $\{\rho^{rs}\}=\{\rho^{rr}\}$ or

$$\{\rho^{rs}\} = \left\{\frac{S^{rs}}{d}\right\} = \left[\left[I_1^{rpf}\right] + \left[I_2^{rpf}\right]\right]\left\{\frac{\tau}{E_s}\right\} +$$
$$+ \left[\left[I_1^{rrf}\right] + \left[I_2^{rrf}\right]\right]\left\{\frac{p_r}{E_s}\right\} = \rho_t\{1\} \quad (20)$$

For a group of three GPRs, Eqs (10) and (14) are equated as $\{\rho^{rs}\}=\{\rho^{rr}\}$ or

$$\{\rho^{rs}\} = \left\{\frac{S^{rs}}{d}\right\} = \left[\left[I_1^{rpf}\right] + 2 \times \left[I_2^{rpf}\right]\right]\left\{\frac{\tau}{E_s}\right\} +$$
$$+ \left[\left[I_1^{rrf}\right] + 2 \times \left[I_2^{rrf}\right]\right]\left\{\frac{p_r}{E_s}\right\} = \rho_t\{1\} \quad (21)$$

Table 1: Validation and comparison of α for groups of two, three, and four GP–GPR systems.

PARAMETERS	SETTLEMENT INTERACTION FACTOR, α	REFERENCES
L/d=10, s/d=3, v_s= 0.5, K_{gp}=10000	0.494	Present analysis for 2GPs
L/d=10, s/d=3, v_s= 0.5, K_{gp}=∞	0.493	Poulos (1968)
L/d=25, s/d=3, v_s= 0.5, K_{gp}=10000	0.584	Present analysis for 2GPs
L/d=25, s/d=3, v_s= 0.5, K_{gp}=∞	0.582	Poulos (1968)
L/d=25, s/d=3, v_s= 0, K_{gp}=10000	0.631	Present analysis for 2GPs
L/d=25, s/d=3, v_s= 0, K_{gp}=∞	0.630	Poulos (1968)
L/d=25, s/d=10, v_s=0.5, K_{gp}=10000	0.299	Present analysis for 2GPs
L/d=25, s/d=10, v_s=0.5, K_{gp}=1000	0.26	Kitiyodom and Matsumoto (2003)
L/d=25, s/d=10, v_s=0.5, K_{gp}=1000	0.265	Present analysis for 2GPs
L/d=25, s/d=10, v_s= 0.5, K_{gp}=∞	0.31	Poulos (1968)
L/d=25, s/d=10, v_s=0.5, K_{gp}=10000	0.596	Present analysis for 3GPs
L/d=25, s/d=10, v_s= 0.5, K_{gp}=∞	0.589	Poulos (1968)
L/d=25, s/d=10, v_s=0.5, K_{gp}=10000	0.829	Present analysis for 4GPs
L/d=25, s/d=10, v_s= 0.5, K_{gp}=∞	0.81	Poulos (1968)
L/d=10, D/d=2, s/d=4, v_s=0.5, K_{gp}=10000	0.42	Present analysis for 2GPRs
L/d=10, D/d=2, s/d=4, v_s=0.5, K_{gp}=∞	0.41	Davis and Poulos (1972)
L/d=10, D/d=2, s/d=6, v_s=0.5, K_{gp}=10000	0.311	Present analysis for 2GPRs
L/d=10, D/d=2, s/d=6, v_s=0.5, K_{gp}=∞	0.31	Davis and Poulos (1972)
L/d=25, D/d=2, s/d=4, v_s=0.5, K_{gp}=10000	0.51	Present analysis for 2GPRs
L/d=25, D/d=2, s/d=4, v_s=0.5, K_{gp}=∞	0.50	Davis and Poulos (1972)
L/d=25, D/d=2, s/d=6, v_s=0, K_{gp}=10000	0.471	Present analysis for 2GPRs
L/d=25, D/d=2, s/d=6, v_s=0, K_{gp}=∞	0.47	Davis and Poulos (1972)

For a group of four GPRs, Eqs (12) and (14) are equated as $\{\rho^{rs}\}=\{\rho^{rr}\}$ or

$$\{\rho^{rs}\} = \left\{\frac{S^{rs}}{d}\right\} = \left[\left[I_1^{rpf}\right] + 2\times\left[I_2^{rpf}\right] + \right.$$
$$\left. + \left[I_4^{rpf}\right]\right]\left\{\frac{\tau}{E_s}\right\} + \left[\left[I_1^{rrf}\right] + 2\times\left[I_2^{rrf}\right] + \left[I_4^{rrf}\right]\right]\left\{\frac{p_r}{E_s}\right\} = \rho_t\{1\} \quad (22)$$

The parameter α (SIF) as defined by Solanki and Sharma (2023) is used to analyze the SIF with different non-dimensional variables.

For groups of two, three, and four GPs, α is given as follows:

$$\text{“}\alpha_{2r(GPs)} = \frac{\text{settlement of a GP in a group of two GPs} - \text{settlement of a single GP}}{\text{settlement of single GP}} \quad (23)$$

$$\alpha_{3r(GPs)} = \frac{\text{settlement of a GP in a group of three GPs} - \text{settlement of a single GP}}{\text{settlement of single GP}} \quad (24)$$

$$\alpha_{4r(GPs)} = \frac{\text{settlement of a GP in a group of four GPs} - \text{settlement of a single GP}}{\text{settlement of single GP}}\text{,,} \quad (25)$$

For groups of two, three, and four GPRs, α is given as follows:

$$\text{“}\alpha_{2r(GPRs)} = \frac{\text{settlement of a GPR in a group of two GPRs} - \text{settlement of a single GPR}}{\text{settlement of single GPR}} \quad (26)$$

$$\alpha_{3r(GPRs)} = \frac{\text{settlement of a GPR in a group of three GPRs} - \text{settlement of a single GPR}}{\text{settlement of single GPR}} \quad (27)$$

$$\alpha_{4r(GPRs)} = \frac{\text{settlement of a GPR in a group of four GPRs} - \text{settlement of a single GPR}}{\text{settlement of single GPR}}\text{,,} \quad (28)$$

(“R”) outcomes were those that were attained after using the above-mentioned analysis.

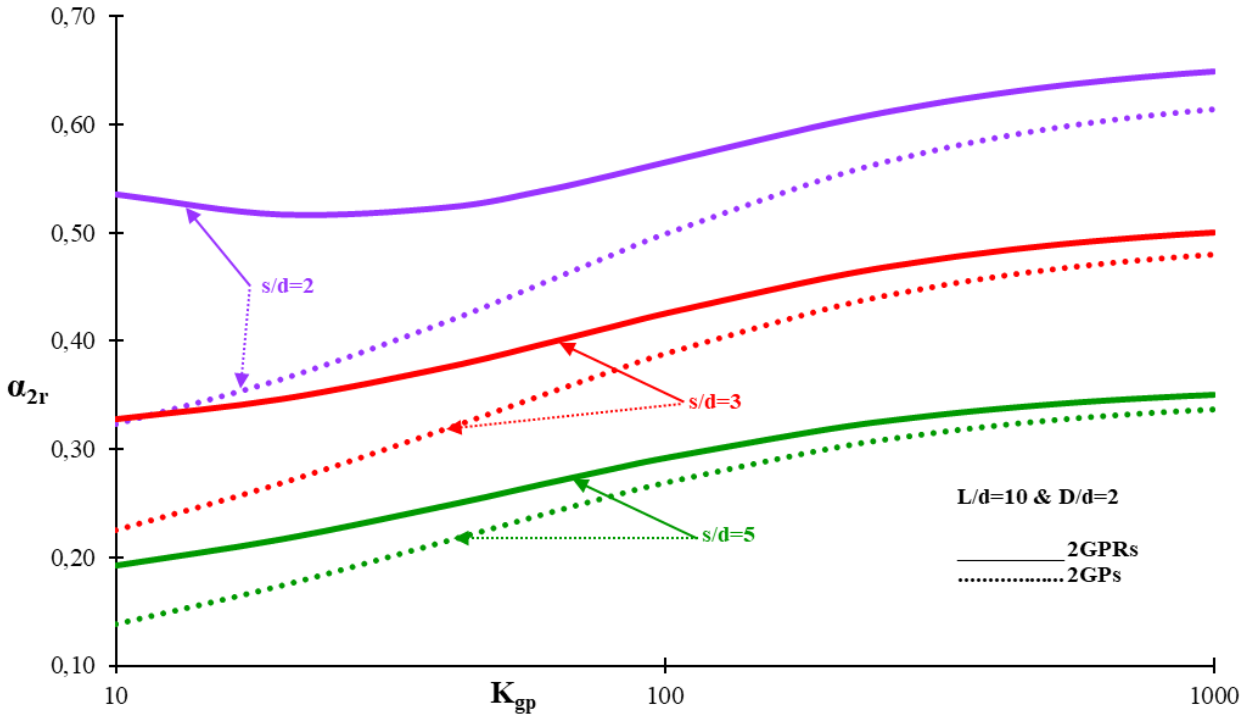

Figure 7: Variation of α_{2r}, with K_{gp}, between 2GPs and 2GPRs—impact of s/d for L/d = 10 and D/d = 2.

Results obtained from the concept of ("S") are given as follows:

$$\alpha_{3s(GPs)} = 2 \times \alpha_2 \quad (29)$$

$$\alpha_{4s(GPs)} = 2 \times \alpha_2 (\text{for spacing, s}) + \alpha_2 (\text{for spacing, } \sqrt{2}\text{s}) \quad (30)$$

$$\alpha_{3s(GPRs)} = 2 \times \alpha_2 \quad (31)$$

$$\alpha_{4s(GPRs)} = 2 \times \alpha_2 (\text{for spacing, s}) + \alpha_2 (\text{for spacing, } \sqrt{2}\text{s}) \quad (32)$$

4 Findings and Discussion

4.1 Verification and Comparison of the Proposed Approach

The research findings in Table 1 were initially compared with the studies conducted by Poulos (1968) and Davis and Poulos (1972) to assess the performance of GPs and GPRs in groups of two, three, and four. Table 1 presents the determined α values for different parameters: L/d = 25, K_{gp} = 10000, s/d = 4, and D/d = 2. As per the analysis conducted by Davis and Poulos and the current study, the α values were found to be 0.50 and 0.51, respectively. The agreement between the recommended approach and the previous studies is evident from their close proximity and a mere 1.98 percent difference in values.

4.2 Parametric Study

The SIF refers to the influence of neighboring piles on the settlement behavior of a particular pile within a group of piles. When multiple granular piles are closely spaced, their individual settlements can be affected by the presence and characteristics of neighboring piles. It is typically determined through analytical methods or numerical simulations that consider the soil–pile interaction and the influence of adjacent piles. By incorporating this factor into settlement calculations, engineers can obtain a more accurate prediction of the settlement behavior of a particular pile in a group.

Fig. 7 shows the variation of α_{2r} for groups of 2GPRs and 2GPs, which is presented against K_{gp}, it may well be noted that α_{2r} increases with the values of K_{gp}. Furthermore, the influence of s/d on the value of α_{2r} is illustrated. Observing the trend, it can be noted that as the value of s/d increases, the value of α_{2r} decreases. This decrease in α_{2r} indicates a decline in the interaction between the piles, which can be attributed to the higher s/d values. Also, it is observed that the value of α is more for 2GPRs instead of 2GPs because in the case of 2GPRs, the load from the superstructure is

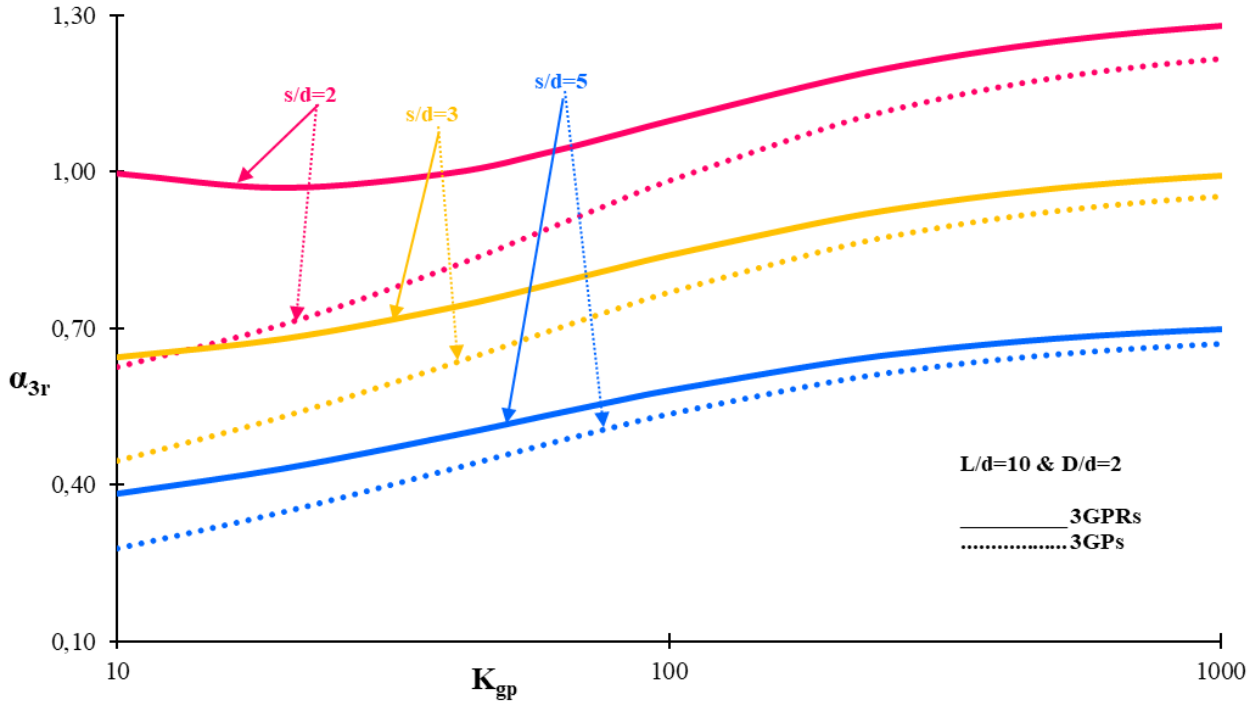

Figure 8: Variation of α_{3r}, with K_{gp}, between the 3GPs and 3GPRs—impact of s/d for L/d = 10 and D/d = 2.

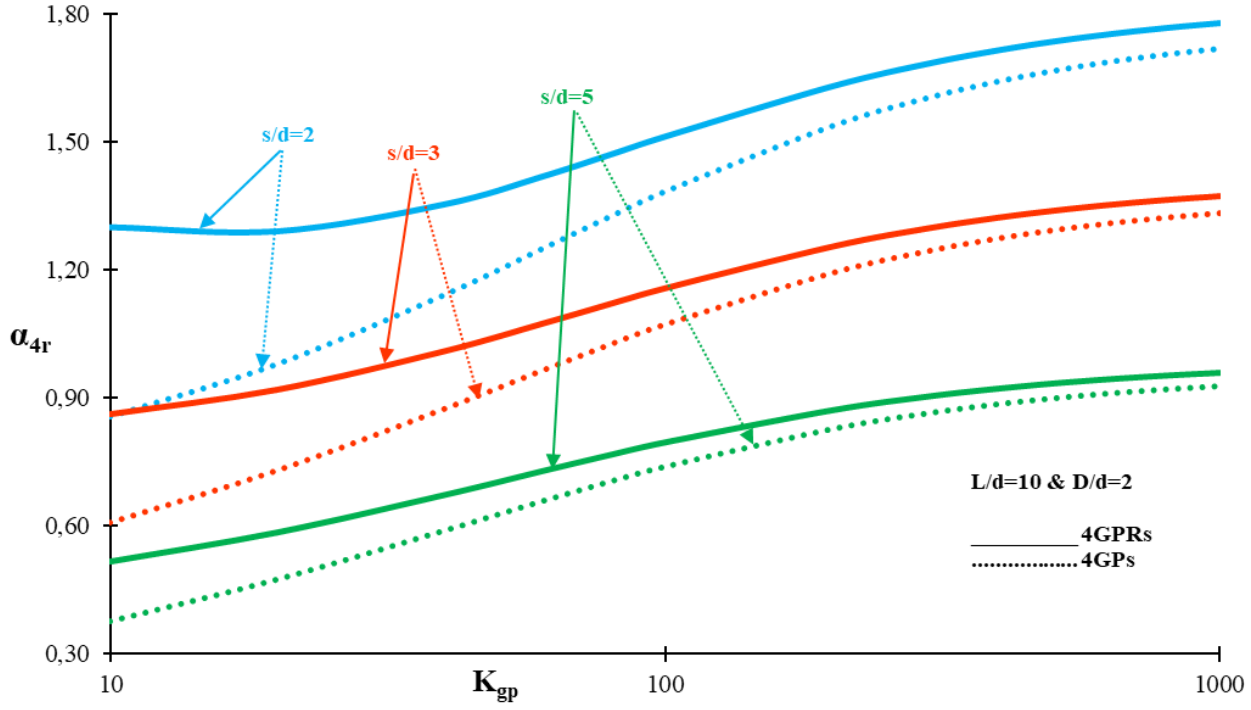

Figure 9: Variation of α_{4r}, with K_{gp}, between 4GPs and 4GPRs—impact of s/d for L/d = 10 and D/d = 2.

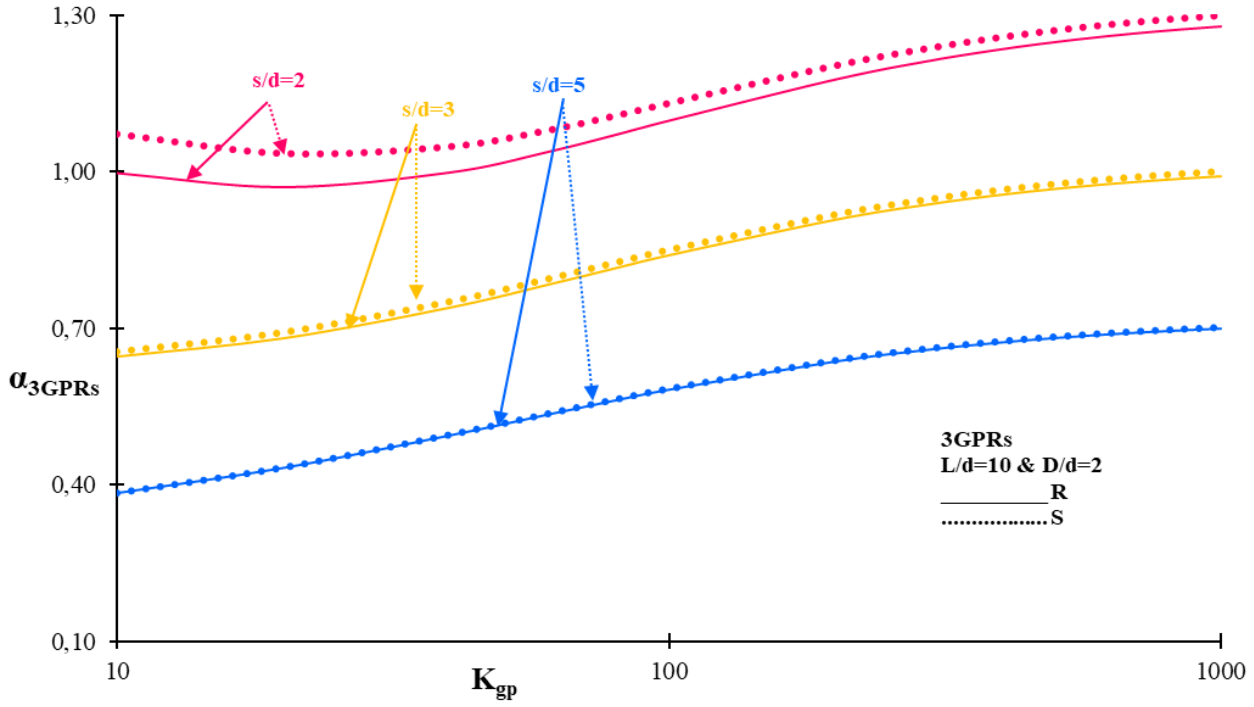

Figure 10: Variation of α_{3GPRs}, with K_{gp}, between the 3GPRs—impact of s/d for L/d = 10 and D/d = 2, R and S analyses.

distributed over a larger area through the raft, leading to a more uniform stress distribution. This helps in reducing the differential settlement between adjacent rafts. On the other hand, individual piles carry the load independently, resulting in localized stress concentrations and potentially higher differential settlements between adjacent piles.

Fig. 8 illustrates the relationship between the variation of α_{3r} for a group consisting of 3GPRs and 3GPs in relation to K_{gp}. It is worth noting that α_{3r} tends to increase as the values of K_{gp} rise. Additionally, the impact of normalized spacing, s/d, on the value of α_{3r} is depicted. It can be observed that as the value of s/d increases, α_{3r} decreases, indicating a decline in interaction between the piles. Consequently, this affects the settlement interaction factor, α_{3r}. A similar trend like Fig. 7 is observed in Fig. 8 except that $\alpha_{3r} > \alpha_{2r}$, and this is because in 3GPRs, the load from the superstructure is distributed among three rafts, resulting in a more even distribution of load and stress across the foundation. This load-sharing mechanism facilitates a reduction in differential settlements among the rafts within the group. On the other hand, in 2GPRs, the load is distributed between only two rafts, which may lead to a less balanced load distribution and potentially higher differential settlements.

Fig. 9 depicts the correlation between the variation of α_{4r} for a group comprising 4GPRs and 4GPs in relation to the relative stiffness of the GP, which is denoted as K_{gp}. It is important to note that as the values of K_{gp} increase, α_{4r} demonstrates a tendency to rise as well because higher K_{gp} indicates that the GP is stiffer and can carry a larger proportion of the load from the superstructure. This increased load-carrying capacity allows for a more even distribution of load among the piles. If GP has a higher relative stiffness, it can transfer a larger portion of the load to the underlying soil. This results in improved load sharing among the piles within the group. Fig. 9 also showcases the influence of normalized spacing, s/d, on the value of α4r. It can be observed that when the value of s/d increases, it results in a decrease in the interaction between the piles and the surrounding soil. With less interaction, there is a reduced transfer of load between the piles and the soil, leading to a decrease in the α. Similar trends to those observed in Fig. 7 and Fig. 8 can be identified in Fig. 9, with the exception that α4r > α3r > α2r, highlighting the higher settlement interaction factor exhibited by the 4GPR configuration than by the 3GPR and 2GPR configurations, and the same implies for GPs.

From Fig. 10, it is evident that the values derived from "R" analysis and those obtained from "S" analysis are very close to each other. This suggests that the rigorous analysis is providing accurate results compared to the superposition method. As the GP becomes stiffer, it can better distribute the load, and this results in reduced settlements for the group of 3GPRs. However, the decrease

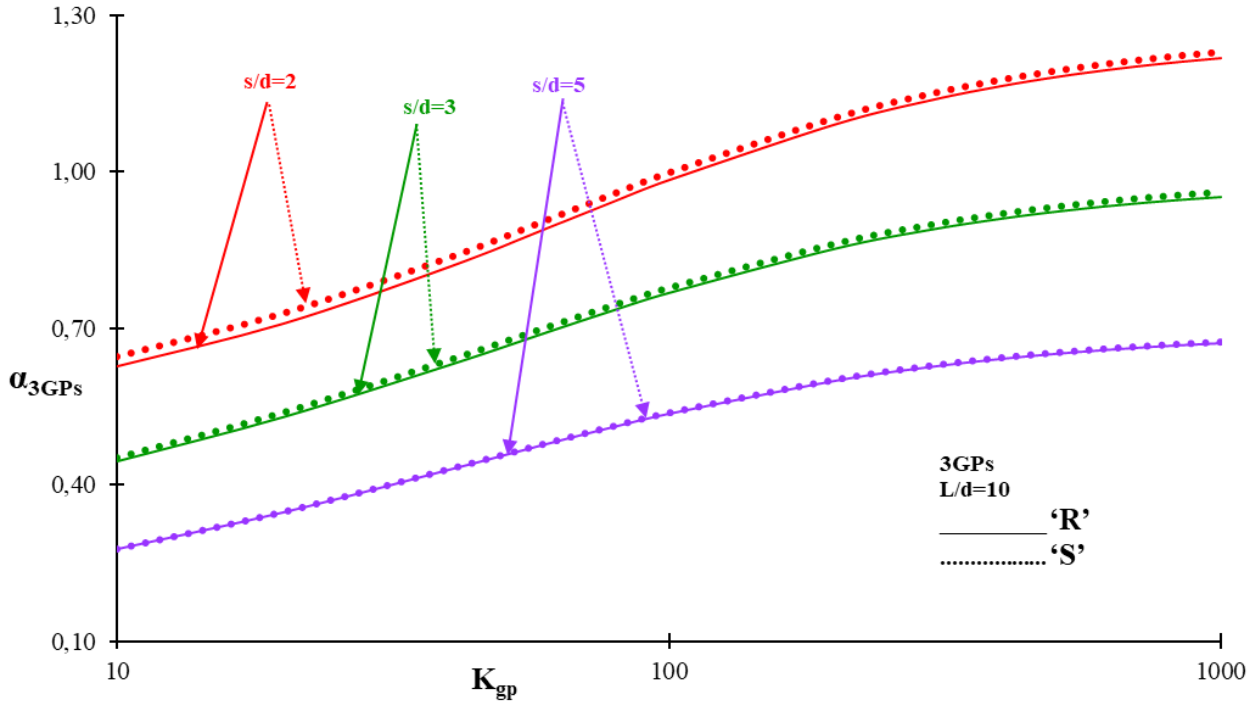

Figure 11: Variation of α_{3GPs}, with K_{gp}, between 3GPs—impact of s/d for L/d = 10, R and S analyses.

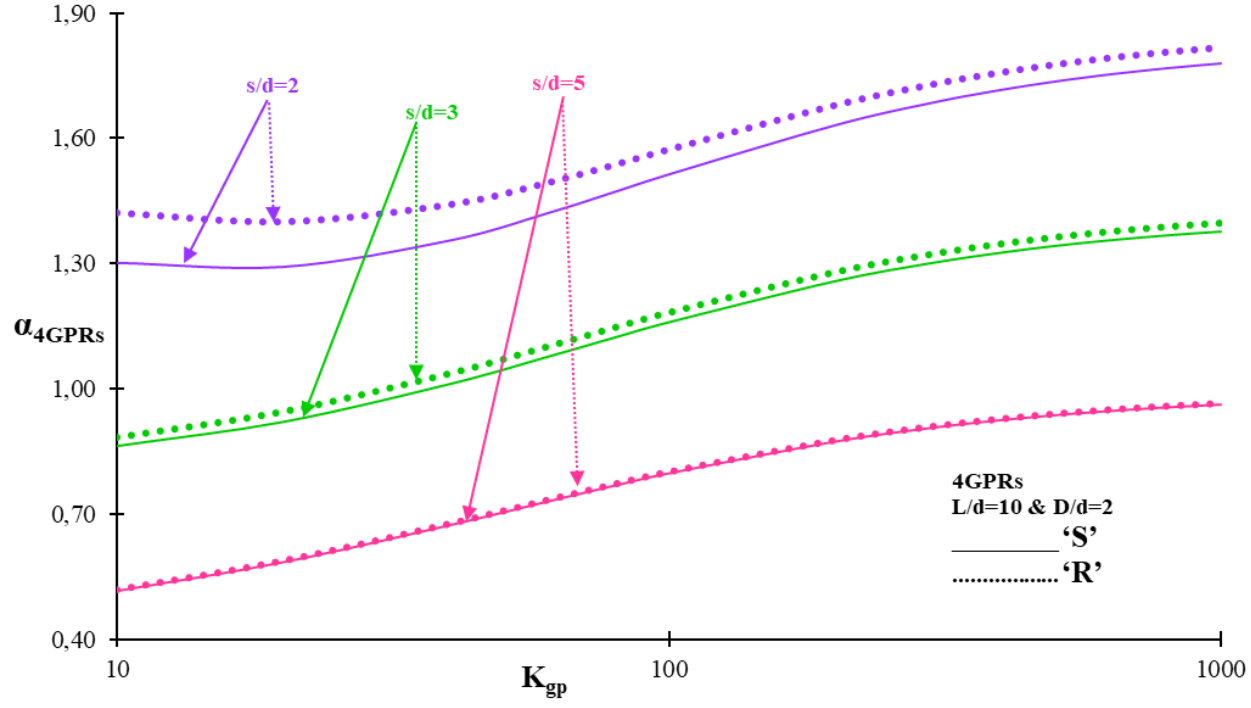

Figure 12: Variation of α_{4GPRs}, with K_{gp}, between 4GPRs—impact of s/d for L/d = 10 and D/d = 2, R and S analyses.

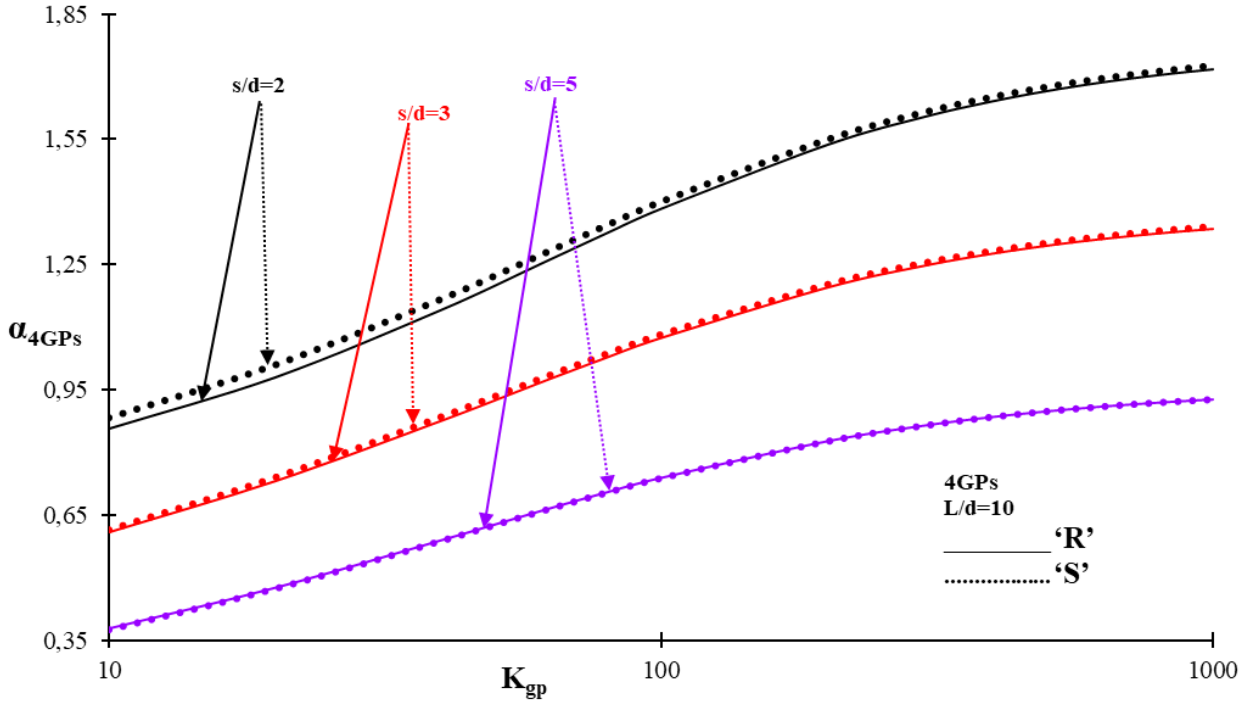

Figure 13: Variation of α_{4GPs}, with K_{gp}, between 4GPs—impact of s/d for L/d = 10, R and S analyses.

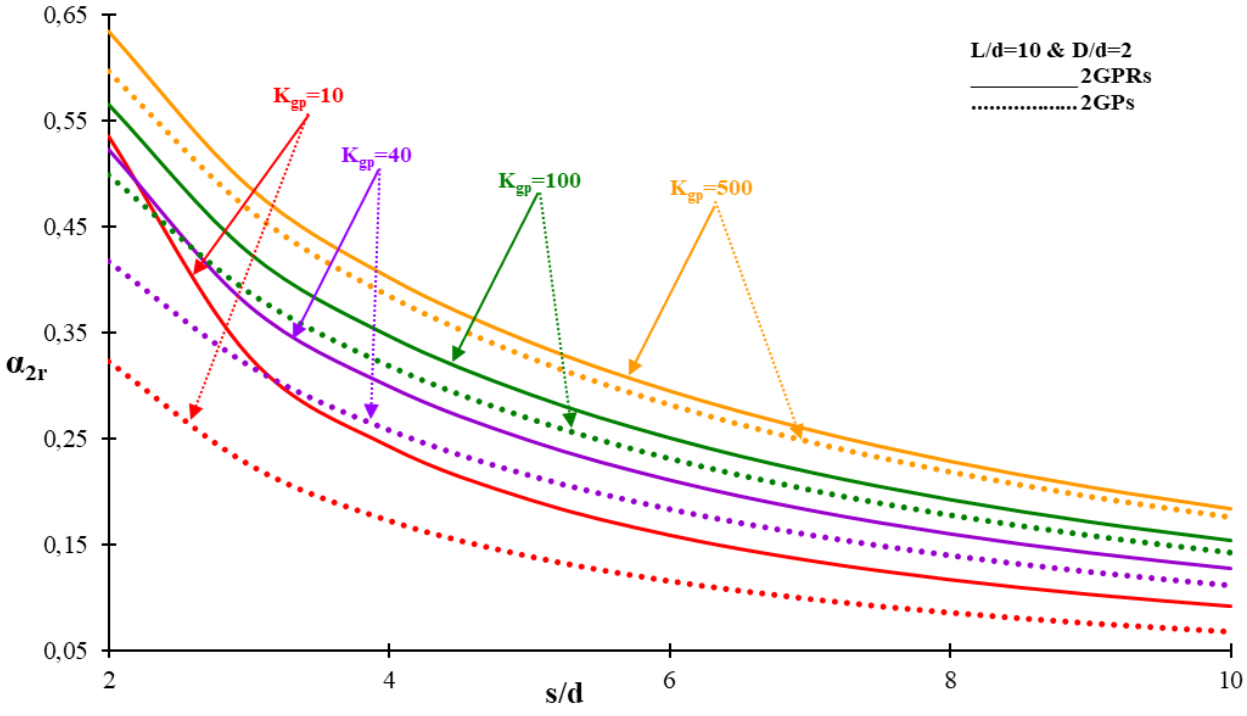

Figure 14: (a) α_{2r} v/s s/d, between 2GPRs and 2GPs—impact of K_{gp} for L/d = 10 and D/d=2.

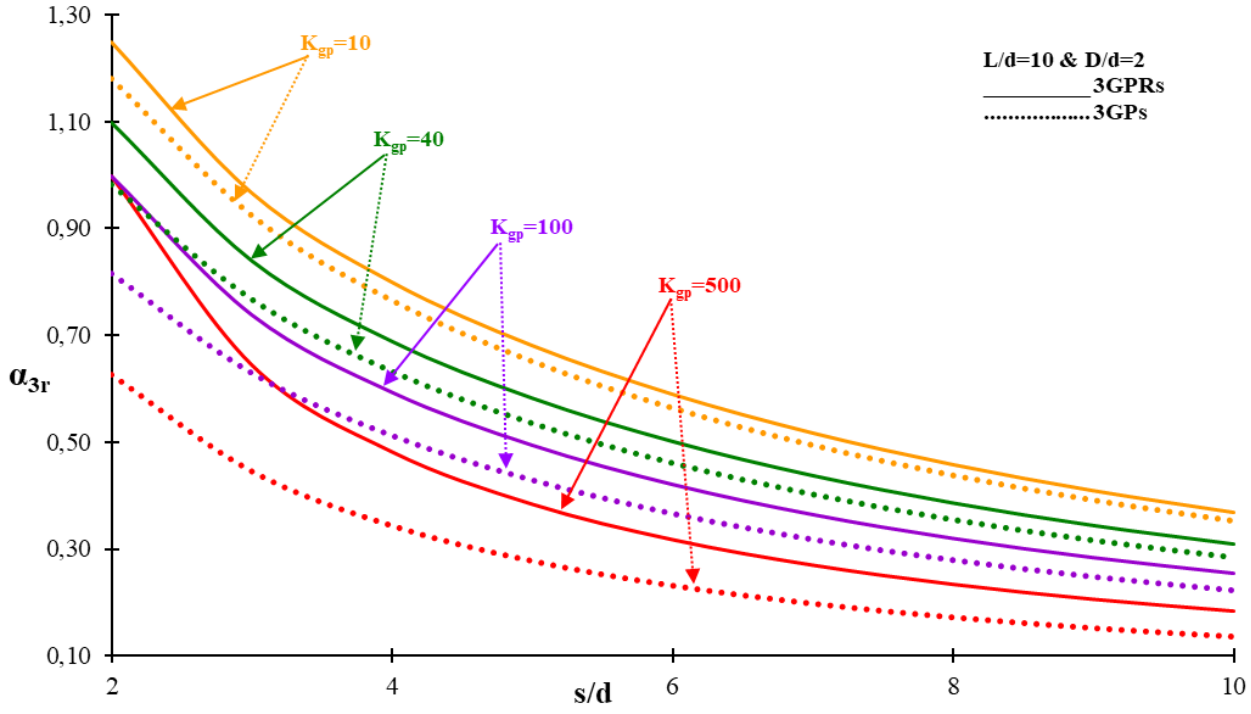

Figure. 14 (b): α_{3r} v/s s/d, between 3GPRs and 3GPs—impact of K_{gp} for L/d = 10 and D/d=2.

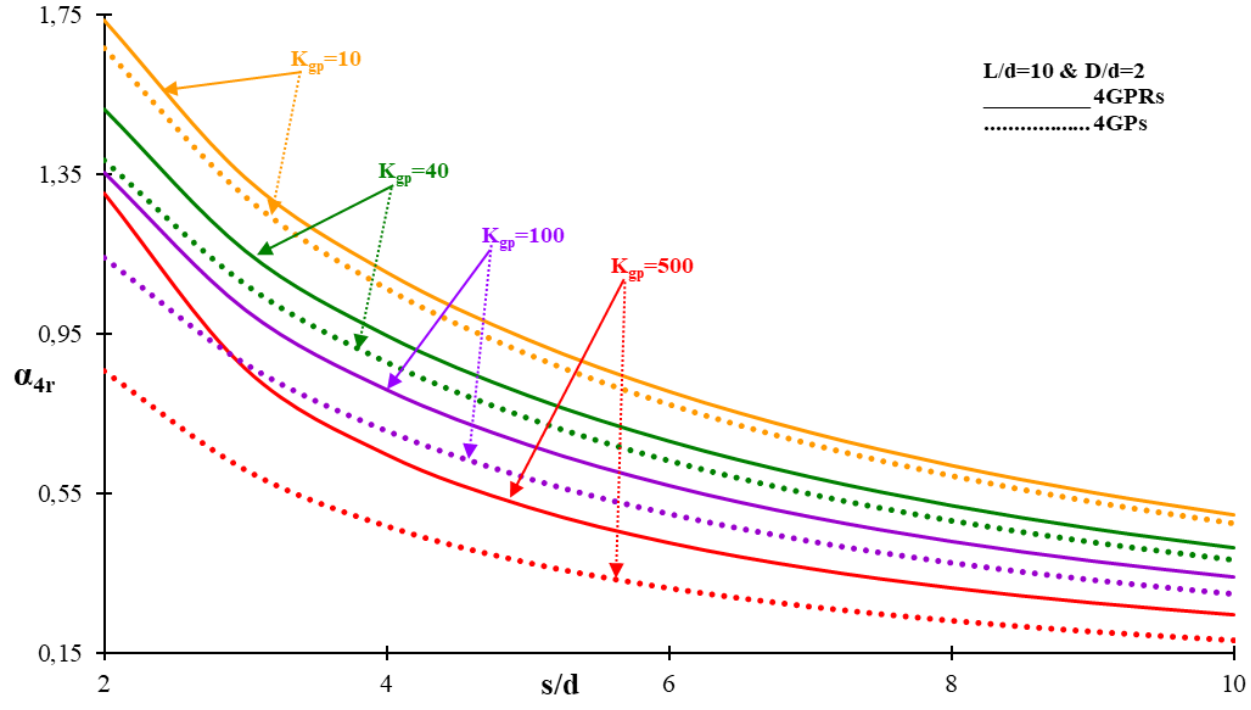

Figure 14: (c) α_{4r} v/s s/d, between 4GPRs and 4GPs—impact of K_{gp} for L/d = 10 and D/d=2.

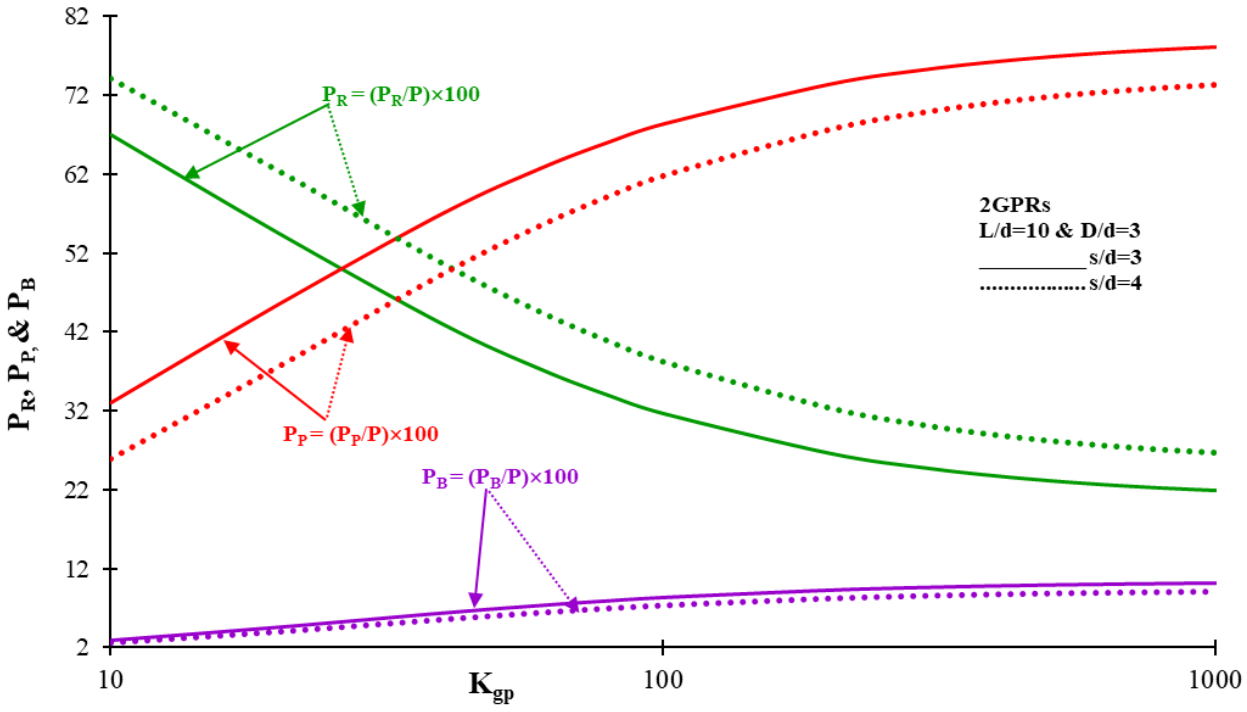

Figure 15 (a): Changes in P_R, P_P, and P_B with respect to total load with K_{gp} for 2GPRs—impact of s/d = 3 and 4 for L/d = 10 and D/d = 3.

in settlement for each individual piled raft is relatively larger than the decrease in the overall settlement of the group. As a consequence, the settlement interaction factor α_{3GPRs} increases, indicating a stronger interaction and interdependence between the piled rafts within the group.

Fig. 11 depicts the correlation between the variation of α_{3GPs} for a group comprising 3GPs in relation to K_{gp}, considering both "R" and "S" analyses. Trend is similar to that of Fig. 10, except $\alpha_{3GPs} < \alpha_{3GPRs}$, because the presence of an additional raft in 3GPRs increases the overall contact area with the underlying soil. This larger contact area enhances the soil–raft interaction, allowing for a more efficient load transfer and reducing the potential for differential settlements. In contrast, 2GPRs have a smaller contact area, limiting the interaction with the soil and potentially leading to less effective load distribution.

The behaviour of 4GPR for both R" analysis and "S" results in Fig. 12 supports the accuracy of the rigorous analysis method. Furthermore, the increase in α_{4GPRs} with higher K_{gp} demonstrates the enhanced load distribution and interaction between the GPRs. Also, as the s/d between the GPRs increases, the interaction between the rafts diminishes. With larger spacing, the influence of one raft on another decreases, leading to a reduction in the interdependence and interaction between the rafts. Consequently, the "S" method, which assumes independent behavior of the rafts, becomes more applicable and provides results closer to those obtained from rigorous analysis.

Fig. 13 illustrates the relationship between the variation of α_{4GPs}, representing a group of 4GPs, and the K_{gp}. The analysis considers both "R" and "S" methods. The trend observed in Fig. 13 is similar to that in Fig. 12, with one key difference: $\alpha 4_{GPs} < \alpha_{4GPRs}$, and the reason behind this discrepancy is that the presence of an additional raft in a group of 4GPRs increases the overall contact area with the underlying soil. This larger contact area enhances the interaction between the soil and the rafts, resulting in a more efficient transfer of loads and a reduced potential for differential settlements, as a result, the settlement interaction factor of α_{4GPs} is lower than that of α_{4GPRs}.

Variations of α_{2r}, α_3, and α_{4r} with "s/d" of GPs are depicted in Fig. 14 (a), (b), and (c) for D/d = 3, L/d = 10, and K_{gp} = 10, 40, 100, and 500. The rate at which α_{2r} decreases becomes more rapid as s/d increases. This phenomenon occurs because at higher s/d values, the behavior of the 2GPRs tends to resemble that of a GPR. As a result, the interaction between the individual rafts becomes significantly reduced. With larger s/d values, the spacing between the 2GPRs becomes more significant than their individual sizes. Also, the value of α_{2r} for K_{gp} = 40 is comparatively less than that for K_{gp} = 500 because as K_{gp} increases, it becomes more capable of distributing the load more evenly among the piled rafts. This improved

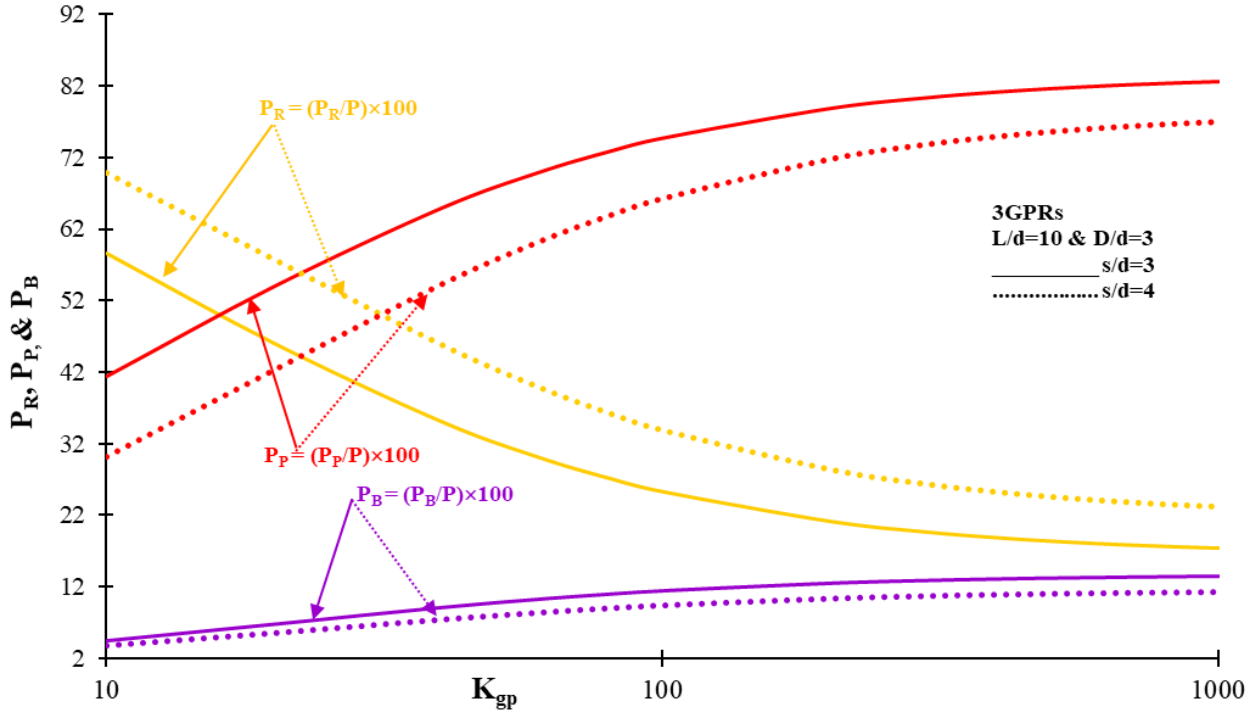

Figure 15 (b): Changes in P_R, P_P, and P_B with respect to total load with K_{gp} for 3GPRs—impact of s/d = 3 and 4 for L/d = 10 and D/d = 3.

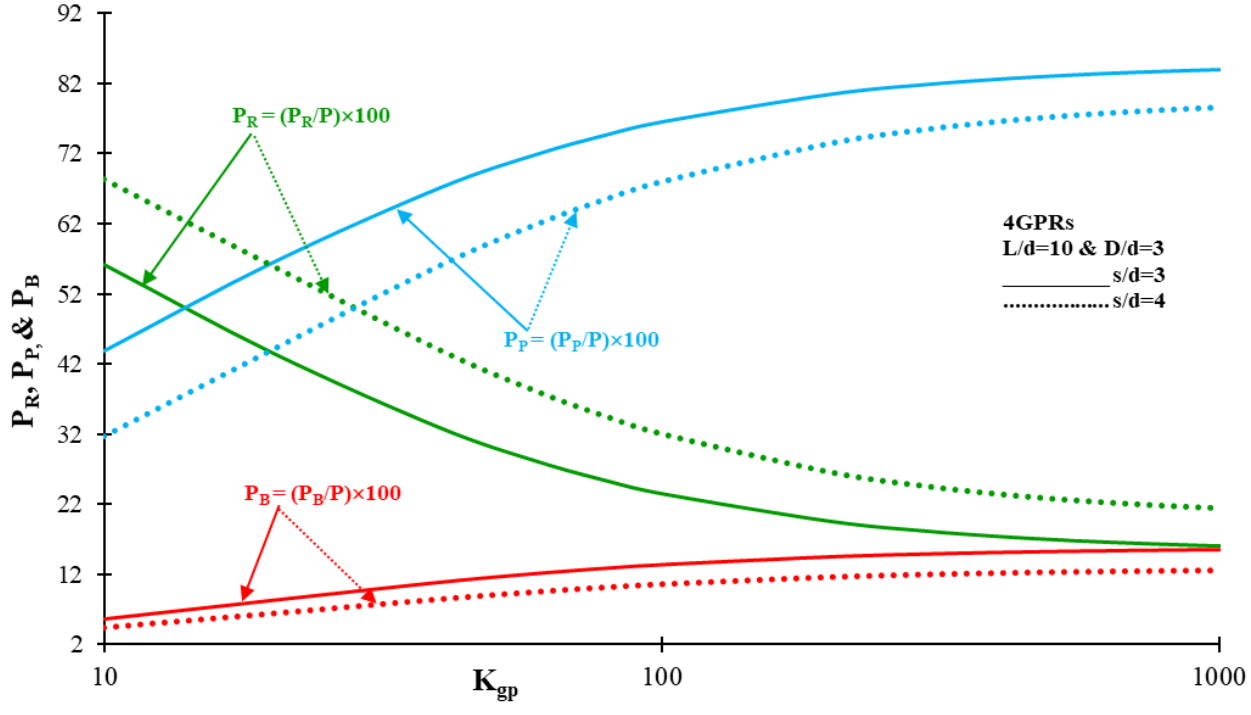

Figure 15 (c): Changes in P_R, P_P, and P_B with respect to total load with K_{gp} for 4GPRs—impact of s/d = 3 and 4 for L/d = 10 and D/d = 3.

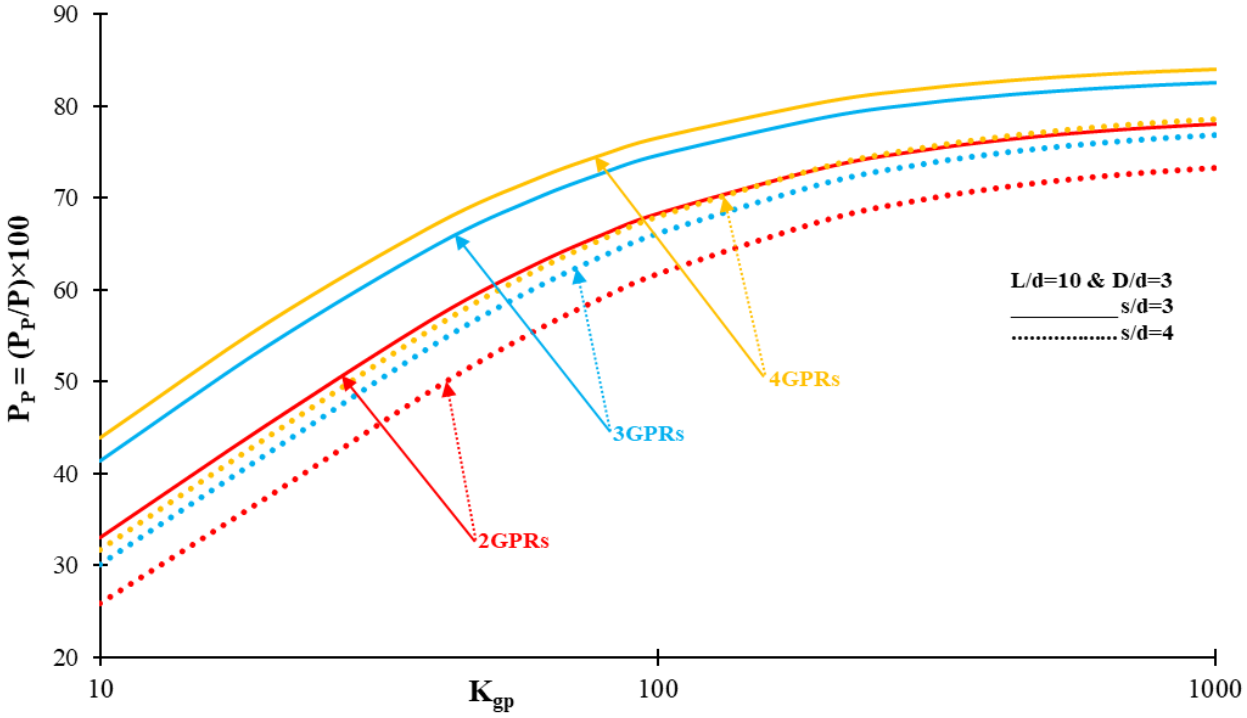

Figure 16: Changes in P_p with respect to total load with K_{gp} for 2GPRs, 3GPRs, and 4GPRs—impact of s/d = 3 and 4 for L/d = 10 and D/d = 3.

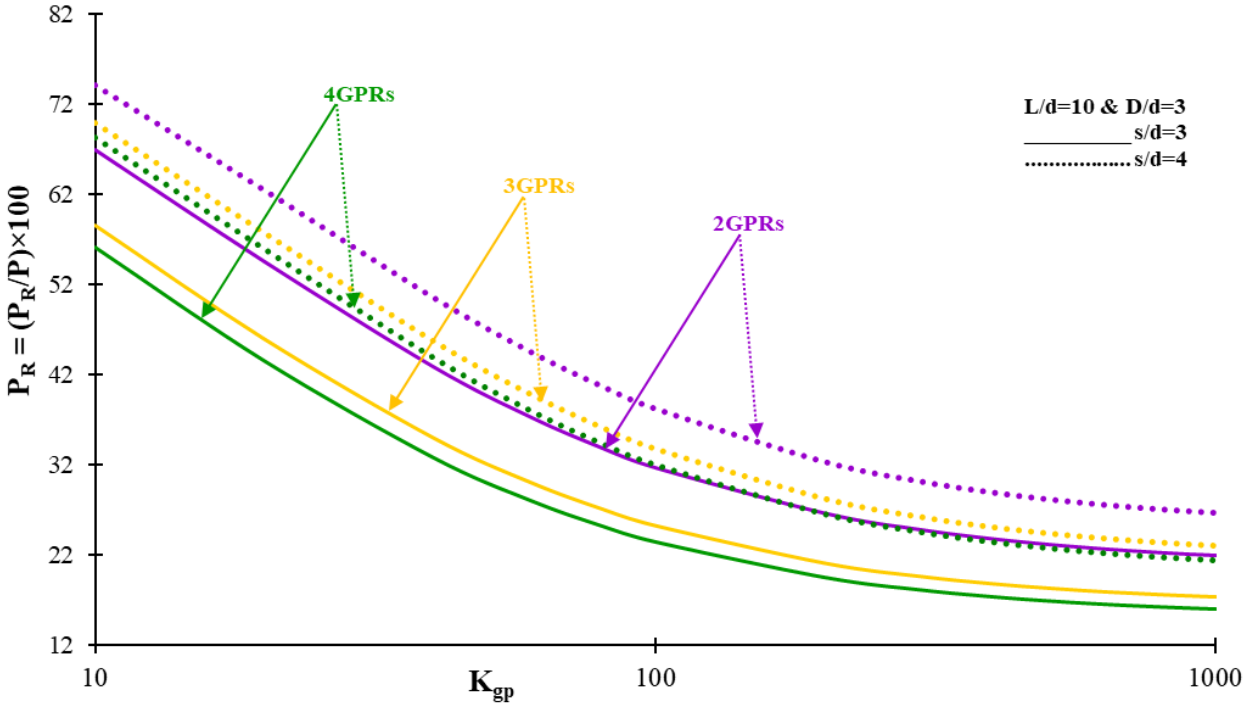

Figure 17: Changes in P_R with respect to total load with K_{gp} for 2GPRs, 3GPRs, and 4GPRs—impact of s/d = 3 and 4 for L/d = 10 and D/d = 3.

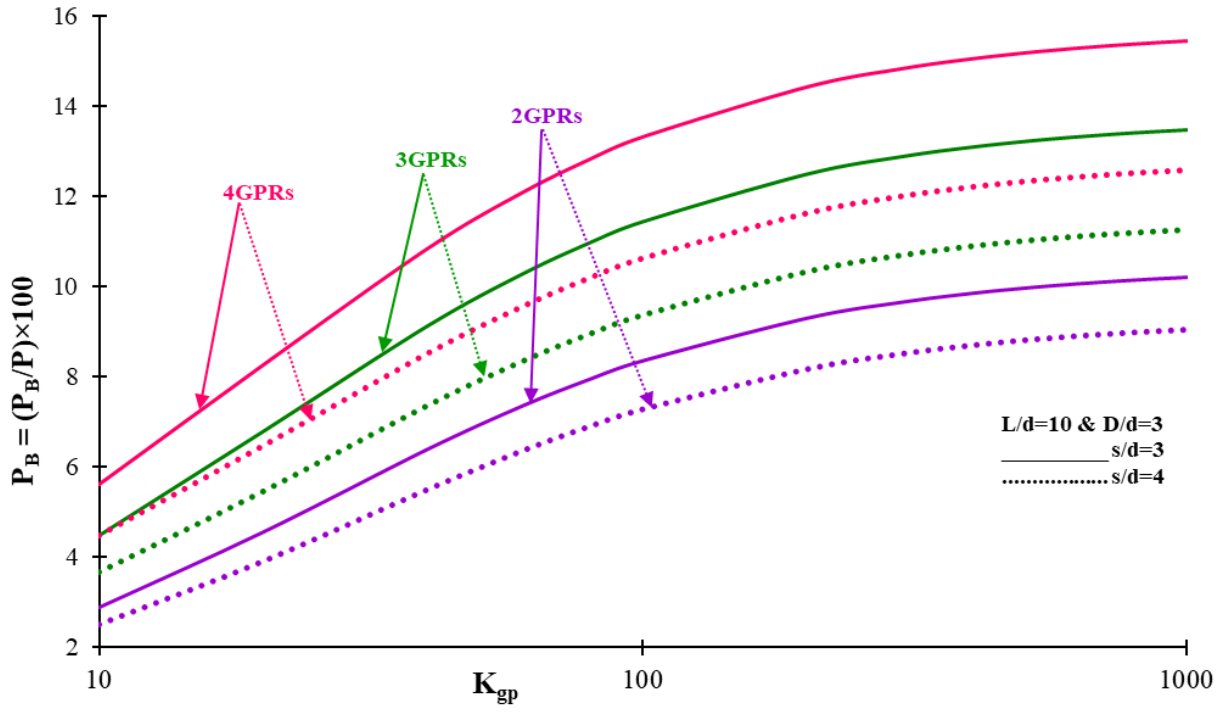

Figure 18: Changes in P_B with respect to total load with K_{gp}, for groups of 2GPRs, 3GPRs, and 4GPRs—impact of s/d = 3 and 4 for L/d = 10 and D/d = 3.

load distribution results in reduced settlements for the group of rafts as a whole. However, the decrease in settlement for each individual raft is relatively smaller than the overall settlement of the group. Consequently, the relative decrement in settlement for the individual raft becomes less significant, leading to an increase in the α_2. A similar trend is observed in Fig. 14 (b) and (c), and only difference is $\alpha_{2r} < \alpha_3 < \alpha_{4r}$.

Fig. 15 (a), (b), and (c) presents the variations in fractional raft load, pile load, and base load for a scenario with L/d = 10 and D/d = 3 for groups of 2GPRs, 3GPRs, and 4GPRs, respectively. The illustration also considers the K_{gp} and illustrates the influence of the s/d between 2GPRs, denoted as s/d. The fractional raft load, $(P_R/P)\times100$, represents the percentage of the total load carried by the raft. The fractional pile load, $(P_p/P)\times100$, represents the percentage of the total load carried by the individual piles. The fractional base load, $(P_B/P)\times100$, represents the percentage of the total load transferred to the underlying soil. The fractional load of a raft and the fractional load of a pile exhibit an inverse relationship, as in piled raft foundation, the load from the superstructure is transmitted to both the raft and the individual piles. The raft, being a larger and more rigid element, is capable of distributing a significant portion of the load over a wider area. As a result, the raft carries a larger proportion of the total load applied to the system. On the other hand, the individual piles, being smaller and more flexible than the raft, carry a smaller portion of the total load. Their load-carrying capacity is primarily dependent on their individual stiffness, hence with increase of K_{gp} load carried by piles and base increases and for raft it decreases. A similar trend is observed in Fig. 15 (b) and (c), but the only difference is the fractional loads with respect to total load: 4GPRs > 3GPRs > 2GPRs.

For L/d = 10 and D/d = 3, Fig. 16 illustrates the variation of $(P_p/P)\times100$ with K_{gp} of GP considering the effect of s/d = 3 and 4. As shown in Fig. 16, $(P_p/P)\times100$ is more for 4GPRs > 3GPRs > 2GPRs because in 4GPRs, there are more piles in total than the groups with two or three rafts. With more piles, the load from the superstructure is distributed among a larger number of load-bearing elements. As a result, each individual pile carries a smaller portion of the total load, leading to a higher percentage load carried by each pile. Also, there will be an enhanced load transfer because the presence of more piles in 4GPRs allows for a greater number of load transfer paths. The additional piles increase the load-sharing capacity within the foundation system, enabling a more efficient transfer of the applied load from the superstructure. This improved load transfer reduces the load carried by each individual pile and contributes to a higher percentage load carried by the pile.

Table 1: Calculated α Values for 2GPR, 3GPR, and 4GPR at Different K_{gp} Values.

K_{gp}	$S_{single\ GPR}$	S_{2GPRs}	α_2	S_{3GPRs}	α_3	S_{4GPRs}	α_4
10	0.28896019	0.44372244	0.5354	0.57710092	0.9974	0.66499219	1.3012
20	0.24921961	0.37804292	0.517	0.4909663	0.9707	0.57116472	1.2923
40	0.21146596	0.32215436	0.5237	0.42253469	0.9977	0.49794194	1.3545
60	0.19295914	0.29693231	0.5392	0.3930989	1.037	0.46686672	1.4202
80	0.18191326	0.28252547	0.5527	0.37668362	1.0703	0.44965581	1.4722
100	0.17456244	0.27319766	0.5653	0.36620857	1.0974	0.43871883	1.5138
200	0.15786745	0.25275908	0.6007	0.34367319	1.1776	0.41531357	1.6311
300	0.15160321	0.24534996	0.6177	0.33564417	1.2138	0.40701624	1.6848
400	0.14831981	0.24152163	0.6284	0.33152454	1.2357	0.40276757	1.7154
500	0.14629833	0.23918332	0.6355	0.32901799	1.2489	0.40018538	1.7365
600	0.1449285	0.23760681	0.6402	0.32733219	1.2588	0.39844994	1.7517
700	0.14393894	0.23647197	0.6434	0.32612074	1.2667	0.39720341	1.7627
800	0.1431906	0.23561598	0.6455	0.3252081	1.2727	0.3962647	1.7703
900	0.14260485	0.23494732	0.6468	0.32449587	1.2774	0.39553232	1.7757
1000	0.14213391	0.23441055	0.6476	0.32392456	1.2811	0.39494498	1.7797

Besides this, the interaction between adjacent piles in a group of four granular piled rafts can also contribute to a higher percentage load carried by the pile. The presence of neighboring piles helps to distribute the load and alleviate localized stress concentrations. This interaction effect leads to a more uniform distribution of the load among the individual piles, resulting in a higher percentage load carried by each pile.

Fig. 17 presents the relationship between $(P_R/P)\times100$, which represents the fractional raft load, and K_{gp} of the GP for a scenario with L/d = 10 and D/d = 3. The figure also considers the impact of s/d = 3 and 4, denoting the spacing between the granular piled rafts. From Fig. 17, it can be observed that the fractional raft load, $(P_R/P)\times100$, is higher for configurations with a lesser number of GPRs. In particular, the trend demonstrates a decrease in the fractional load of the raft in the following order: 2GPRs > 3GPRs > 4GPRs. When comparing groups of granular piled rafts, it is more common for the percentage load carried by the raft to decrease as the number of rafts increases. This is because with a greater number of rafts, there are more load-bearing elements (piles or rafts) in the system, which leads to a more distributed load-sharing mechanism. As a result, the load is distributed among the individual piles and rafts, reducing the proportion of load carried by the raft. In contrast, a group of two granular piled rafts may have a higher percentage load carried by the raft because there are fewer load-bearing elements to share the load. This results in a greater proportion of the load being carried by the raft compared to the individual piles.

Fig. 18 depicts the correlation between the fractional base load, $(P_B/P)\times100$, and the relative stiffness, K_{gp}, of the GP for a given scenario with L/d = 10 and D/d = 3. The figure also considers the influence of s/d = 3 and 4, representing the spacing between the GPRs. From Fig. 18, it is evident that the fractional base load, $(P_B/P)\times100$, tends to be higher for configurations with a larger number of GPRs. Specifically, the trend shows that the fractional base load decreases in the following order: 4GPRs > 3GPRs > 2GPRs. It is because of increased load redistribution as in a group of four granular piled rafts, there are more load-bearing elements, including both the rafts and the individual piles. This increased number of load-bearing elements allows for a more distributed load-sharing mechanism. As a result, the load is redistributed among the individual piles and rafts, potentially leading to a higher percentage of the load being carried by the base of the pile. Also, the group 4GPRs have a larger contact area with the underlying soil than groups 2GPRs and 3GPRs. This larger contact area allows for a more efficient load transfer and improves load-carrying capacity at the base of the pile.

5 Example for Calculation Part

Calculations take into account the geometric ratios L/d=10, D/d=2, and s/d=2, which were kept constant throughout the analysis.

For a representative case of K_{gp}=10:

- The settlement of a single GPR was found to be $S_{single\ GPR}$=0.28896019
- For two GPRs: S_{2GPR}=0.443722435, yielding α_2= (0.443722435-0.288960190)/0.288960190 = 0.5354
- For three GPRs: S_{3GPR}=0.577100919, yielding α_3= (0.577100919-0.288960190)/0.288960190 = 0.9974
- For four GPRs: S_{4GPR}=0.664992185, yielding α_4= (0.664992185-0.288960190)/0.288960190 = 1.3012

As shown in Table 1, the settlement interaction factor increases with the number of GPRs in the group. For instance, at K_{gp}=10, α_2 is 0.5354, indicating that placing two GPRs together leads to a settlement increase of approximately 53.5% compared to a single GPR. Similarly, α_3 and α_4 rise to 0.9974 and 1.3012, respectively, demonstrating that larger groups of GPRs result in greater settlement interaction.

This trend holds across all K_{gp} values, where the α_4 values exceed α_3, which in turn exceed α_2. This consistent increase is attributed to the growing influence of group effects as the number of GPRs increases, which leads to a larger combined load and thus higher settlements.

6 Conclusions

In summary, our analysis, rooted in the elastic continuum approach and utilizing Mindlin's equations to incorporate both groups of granular piles and granular piled rafts, has provided valuable insights into the settlement interaction behavior. The comparison between "R" and "S" analyses reveals a consistent trend, albeit with a minor discrepancy that diminishes as the relative stiffness (K_{gp}) increases.

Key Findings:

a) Settlement Interaction Factor Discrepancy: Notably, the settlement interaction factor for granular piled rafts (GPRs) tends to be higher than that of individual granular piles (GPs). This difference arises from the distinct load distribution and soil–structure interaction in the two cases. While individual granular piles operate independently with limited interaction restricted to the soil between them, the proximity of rafts in a group introduces interference effects. Neighboring rafts influence each other, causing soil displacements and inducing changes, resulting in a higher settlement interaction factor for GPRs.

b) Effect of Relative Stiffness (K_{gp}): The settlement interaction factor increases with an elevation in the relative stiffness of granular piles. Higher relative stiffness indicates a stiffer pile, capable of transmitting a larger proportion of the load to the underlying soil. This enhanced load transfer capacity leads to a more efficient distribution of load among the piles within the group, subsequently reducing the settlement of individual piles and contributing to an increase in the settlement interaction factor (α).

c) Spacing-to-Diameter Ratio (s/d) Influence: The settlement interaction factor demonstrates a decrease with an increase in the normalized spacing between granular piles. As the s/d (spacing-to-diameter) ratio enlarges, the distance between piles within the group increases. This results in a decrease in the interaction between piles and the surrounding soil. Reduced interaction leads to a diminished transfer of load between the piles and the soil, causing a decrease in the settlement interaction factor (α).

d) Practical Design Implications: The derived design charts of non-dimensional parameters offer practical utility in the field for an efficient foundation design. These charts facilitate quick and accurate decision making, enhancing the design process for practitioners.

In conclusion, our systematic analysis enhances the understanding of settlement interactions in granular piles and granular piled rafts. The quantifiable trends observed provide a basis for informed design decisions and underscore the practical applicability of the derived parameters.

Data Availability Statement

Some or all data, models, or codes that support the findings of this study are available from the corresponding author on reasonable request.

Author Contributions

Ashish Solanki and Jitendra Kumar Sharma formulated the original idea. Ashish Solanki performed the analysis by validating and comparing the work from the cited literature. Ashish Solanki wrote the manuscript with the help of Jitendra Kumar Sharma and extended the work as per his instructions.

Acknowledgments

The first author is highly grateful to the late Dr. Vaibhaw Garg and would like to acknowledge the suggestions and discussion. His appreciation and positive attitude about the research work have played a significant role. Author is also grateful to Emeritus Prof. M. R. Madhav for his valuable guidance.

Funding

No funding was received to assist with the preparation of this manuscript.

Conflict of Interest Statement

The authors declare that there is no conflicts of interest.

About Authors

Dr. Ashish Solanki completed his PhD from Department of Civil Engineering (Geotechnical Engineering) at Rajasthan Technical University, Kota. He obtained his MTech degree in Geotechnical Engineering from RTU, Kota, in 2018 with Hons. He has research interests in ground improvement technique, numerical and mathematical modeling, stabilization techniques, and deep foundation. He has co-guided 01 MTech student. He has authored 14 papers (9 papers in SCI indexed journals and 4 in Scopus indexed conferences) and 1 granted patent. He also served as a Student Member of American Society of Civil Engineers and also was the reviewer of International Foundations Congress and Equipment Expo (IFCEE21) held in Dallas, Texas, published by ASCE. Recently his paper "Analytical Evaluation of Settlement and Interaction of Floating Granular Piled Rafts Units in Group" published in Indian Geotechnical Journal Volume 53, pages 1309–1337, (2023) was adjudged as the best paper on "Deep Foundations" and was awarded IGS-Kochi Chapter Young Geotechnical Engineer Award held at IGC 2024 MIT, Chhatrapati Sambhajinagar . At present he is currently working as an Assistant Professor at Manda Institute of Technology.

Dr. Jitendra Kumar Sharma is currently working as a Director at Bundelkhand Institute of Engineering & Technology, Jhansi and Professor and HOD in Department of Civil, Petroleum, and Petrochemical Engineering at Rajasthan Technical University, Kota, and serving since 1990. He obtained his PhD degree in Geotechnical Engineering from IIT, Kanpur, in 2000. He is an active researcher with research interests that include ground improvement technique, numerical and mathematical modeling, ANN, soil–structure interaction, stabilization techniques, and deep foundation. He is guiding 13 PhD (8 awarded) and more than 16 MTech students. He has authored more than 100 papers (49 papers in SCI indexed and referred journals and 49 in Scopus indexed conferences) and 3 granted patents. He is currently serving as a life member of Indian Geotechnical Society, Indian Society for Technical Education, and Indian Grade Drawing, Maharashtra, and also a reviewer of Elsevier and Springer Journals. He addressed several lectures and key note address on Recent Advances in Geotechnical Engineering at MITS, Gwalior. He received IGS-Prof. Dinesh Mohan Biannual Prize in 1997 and was selected as a Young Geotechnical Engineer of IGS from India in 2000. Recently, his paper "Effect of Nonlinear Non-homogeneity of Floating Granular Pile and Soil on Settlement" (published in the *Series A Journal of IEI*, Vol. 100, Issue 2) was selected for the subject prize, "Sir Arthur Cotton Memorial," which was presented at the Prize Distribution Ceremony of the 36th Indian Engineering Congress held at Vigyan Bhawan, Maulana Azad Road, New Delhi 110003, on December 26, 2021.

References

[1] Davis, E.H. and Poulos, H.G., 1972. The analysis of pile raft systems. *Australian Geomechanics Journal*, *G2*(1), pp.21-27. https://www.researchgate.net/publication/293124691_ANALYSIS_OF_PILE_RAFT_SYSTEM.

[2] Garg, V., & Sharma, J. K. (2020). Analyses and settlement study of a group of two, three and four partially stiffened floating granular piles. *Geomechanics and Geoengineering*, *15*(3), 203-223. https://doi.org/10.1080/17486025.2019.1635715

[3] Hong, Y. S., Wu, C. S., & Yu, Y. S. (2016). Model tests on geotextile-encased granular columns under 1-g and undrained conditions. *Geotextiles and Geomembranes*, *44*(1), 13-27. https://doi.org/10.1016/j.geotexmem.2015.06.006

[4] Kitiyodom, P., & Matsumoto, T. (2003). A simplified analysis method for piled raft foundations in non-homogeneous soils. International Journal for Numerical and Analytical Methods in Geomechanics, 27(2), 85-109. https://doi.org/10.1002/nag.264

[5] Mattes, N. S., & Poulos, H. G. (1969). Settlement of single compressible pile. *Journal of the Soil Mechanics and Foundations Division*, *95*(1), 189-207. https://doi.org/10.1061/JSFEAQ.0001217

[6] Mindlin, R.D., 1936. Force at a point in the interior of a semi-infinite solid. *physics*, *7*(5), pp.195-202. https://doi.org/10.1063/1.1745385
[7] Mindlin, R.D., 1937. Stress system in a circular disk under radial forces, presented at the joint meeting of applied mechanics and hydraulic division of the ASME held at Cornell University, NY, pp. *A115–118*. https://doi.org/10.1115/1.4008786.
[8] Murugesan, S., & Rajagopal, K. (2006). Geosynthetic-encased stone columns: numerical evaluation. *Geotextiles and Geomembranes*, *24*(6), 349-358. https://doi.org/10.1016/j.geotexmem.2006.05.001
[9] Najjar, S. S., & Skeini, H. (2015). Triaxial response of clays reinforced with granular columns. *Proceedings of the Institution of Civil Engineers-Ground Improvement*, *168*(4), 265-281. https://doi.org/10.1680/grim.13.00049
[10] Poorooshasb, H. B., Miura, N. and Noorzad, A. 1998. An upper bound analysis of the behavior of stone columns. Lecture presented at Saga University, Saga, Japan, pp. 7-37.
[11] Poulos, H.G., 1968. Analysis of the settlement of pile groups. *Geotechnique*, *18*(4), pp.449-471. https://doi.org/10.1680/geot.1968.18.4.449.
[12] Rathor, A. P. S., & Sharma, J. K. (2023). Numerical Evaluation of Settlement and Stresses of Annular Raft. *Journal of The Institution of Engineers (India): Series A*, *104*(1), 187-193. https://doi.org/10.1007/s40030-022-00707-4
[13] Solanki, A., Sharma, J. K., & Madhav, M. R. (2022). Interaction analysis of two floating granular piled raft units. *Geomechanics and Geoengineering*, 1-18. https://doi.org/10.1080/17486025.2022.2136409
[14] Solanki, A., Sharma, J.K. Analytical Evaluation of Settlement and Interaction of Floating Granular Piled Rafts Units in Group. *Indian Geotech J* (2023). https://doi.org/10.1007/s40098-023-00749-w.
[15] Tan, S. A., Tjahyono, S., & Oo, K. K. (2008). Simplified plane-strain modeling of stone-column reinforced ground. *Journal of geotechnical and geoenvironmental engineering*, *134*(2), 185-194. https://doi.org/10.1061/(ASCE)1090-0241(2008)134:2(185)
[16] Zhang, L., & Zhao, M. (2015). Deformation analysis of geotextile-encased stone columns. *International Journal of Geomechanics*, *15*(3), 04014053. https://doi.org/10.1061/(ASCE)GM.1943-5622.0000389